A STATISTICAL VERIFICATION OF A TEN YEAR SERIES OF COMPUTED SURFACE WIND CONDITIONS OVER THE NORTHE PACIFIC AND NORTH ATLANTIC OCEANS

Sigurd Erling Larson

NAVAL POSTGRADUATE SCHOOL
Monterey, California

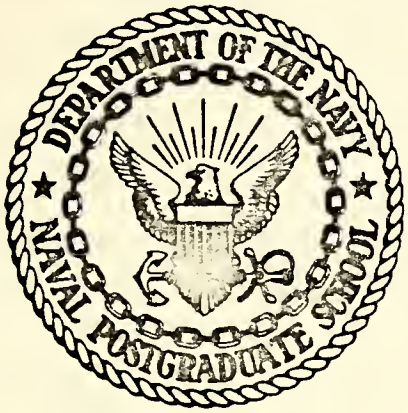

THESIS

A Statistical Verification
of a Ten Year Series of Computed
Surface Wind Conditions Over the
North Pacific and North Atlantic Oceans

by

Sigurd Erling Larson

December 1974

Thesis Advisor: Glenn H. Jung

UNCLASSIFIED

SECURITY CLASSIFICATION OF THIS PAGE *(When Data Entered)*

REPORT DOCUMENTATION PAGE

READ INSTRUCTIONS BEFORE COMPLETING FORM

1. REPORT NUMBER	2. GOVT ACCESSION NO. / 3. RECIPIENT'S CATALOG NUMBER
4. TITLE *(and Subtitle)*: A Statistical Verification of a Ten Year Time Series of Computed Surface Wind Conditions Over the North Pacific and North Atlantic Oceans	5. TYPE OF REPORT & PERIOD COVERED: Master's Thesis, December 1974 / 6. PERFORMING ORG. REPORT NUMBER
7. AUTHOR(s): Sigurd Erling Larson	8. CONTRACT OR GRANT NUMBER(s)
9. PERFORMING ORGANIZATION NAME AND ADDRESS: Naval Postgraduate School, Monterey, CA 93940	10. PROGRAM ELEMENT, PROJECT, TASK AREA & WORK UNIT NUMBERS
11. CONTROLLING OFFICE NAME AND ADDRESS: Naval Postgraduate School, Monterey, CA 93940	12. REPORT DATE: December 1974 / 13. NUMBER OF PAGES
14. MONITORING AGENCY NAME & ADDRESS *(if different from Controlling Office)*	15. SECURITY CLASS. *(of this report)*: Unclassified / 15a. DECLASSIFICATION/DOWNGRADING SCHEDULE

16. DISTRIBUTION STATEMENT *(of this Report)*

Approved for public release; distribution unlimited.

17. DISTRIBUTION STATEMENT *(of the abstract entered in Block 20, if different from Report)*

18. SUPPLEMENTARY NOTES

19. KEY WORDS *(Continue on reverse side if necessary and identify by block number)*

Quasi-Geostrophic Wind	North Pacific Ocean
Computer Model	North Atlantic Ocean
Climatology	Ocean Station Observations
Synoptic Scale	Ten Year Trend

20. ABSTRACT *(Continue on reverse side if necessary and identify by block number)*

The increasing interest in long term (inter-annual) weather changes and their relation to processes in the ocean is beginning to illuminate the need for and the lack of long term records of physically significant variables which occur over the vast oceanic regions of the northern hemisphere. An attempt is made here to evaluate the accuracy of a hindcast time series of surface wind

DD FORM 1 JAN 73 1473 EDITION OF 1 NOV 65 IS OBSOLETE S/N 0102-014-6601

UNCLASSIFIED

SECURITY CLASSIFICATION OF THIS PAGE *(When Data Entered)*

20. Abstract

vector components and speeds for the period of January 1960 through December 1969.

The quasi-geostrophic model used to calculate these records is described as well as the twelve-hourly surface pressure data which were used as input. The central moments of the probability distributions of the computed records are compared to those of corresponding time series observed on Ocean Station Vessels. Linear correlation coefficients between observations and computed records were found to average 0.81 for the components of the wind vector and 0.65 for the wind speed. Regression relations between computed and observed records also are presented. Spectral analysis of low pass filtered records showed coherence between observed and computed records increased with decreasing frequency. The accuracy of the computed records in low latitudes also is estimated.

19. Key Words

Frequency Distribution
Spectra
Correlation
Regression

A Statistical Verification of a Ten Year Series of Computed Surface Wind Conditions Over the North Pacific and North Atlantic Oceans

by

Sigurd Erling Larson
Environmental Prediction Research Facility
B.S., University of Washington, 1968

Submitted in partial fulfillment of the
requirements for the degree of

MASTER OF SCIENCE IN OCEANOGRAPHY

from the

NAVAL POSTGRADUATE SCHOOL
December 1974

ABSTRACT

The increasing interest in long term (inter-annual) weather changes and their relation to processes in the ocean is beginning to illuminate the need for and the lack of long term records of physically significant variables which occur over the vast oceanic regions of the northern hemisphere. An attempt is made here to evaluate the accuracy of a hind cast time series of surface wind vector components and speeds for the period of January 1960 through December 1969.

The quasi-geostrophic model used to calculate these records is described as well as the twelve-hourly surface pressure data which were used as input. The central moments of the probability distributions of the computed records are compared to those of corresponding time series observed on Ocean Station Vessels. Linear correlation coefficients between observed and computed records were found to average 0.81 for the components of the wind vector and 0.65 for the wind speed. Regression relations between computed and observed records also are presented. Spectral analysis of low pass filtered records showed coherence between observed and computed records increased with decreasing frequency. The accuracy of the computed records in low latitudes also is estimated.

TABLE OF CONTENTS

LIST OF TABLES

LIST OF FIGURES

ACKNOWLEDGMENTS

The author wishes to express his gratitude to the Church Computer Center, Naval Postgraduate School; to Fleet Numerical Weather Central for use of their computers and surface pressure data; to David Husby, National Marine Fisheries Service, for use of Ocean Station observational data; to Andrew Bakun, National Marine Fisheries Service for valuable contributions to the formulation of the model; to Dean Dale, Fleet Numerical Weather Central, for a critical review of the model; to Robert Baily, formerly with the Environmental Prediction Research Facility, for his highly competent management of many of the computer runs required; to Professor Edward Thornton who generously provided his spectral analysis program and much valued assistance in its use; and especially to Professor Glenn Jung, faculty advisor, for his patient guidance throughout what must have seemed an interminable undertaking.

I INTRODUCTION

A. GENERAL

One of the most important variables encountered in the study of physical oceanography and air-sea interaction is the wind field at the sea surface. To a large degree, the surface wind velocity and its variability, both in time and space, determine the exchange of heat and momentum across the air-sea interface. Through such exchange the wind affects not only oceanic surface phenomena, such as waves and surface currents, but also features within the sea such as the vertical thermal structure and deep currents.

The smallest scale of concern in this study is the synoptic scale. Such a scale covers a period of time from several hours to several days and a distance from several tens of kilometers to several hundred kilometers. Past attempts at estimating the surface wind field on this scale have been of two types. One could either average wind observations collected over a given area for a specified period of time (Seckel, 1970) or one could estimate the surface winds from a similar collection of observations of other variables, such as surface atmospheric pressure (Roden, 1974).

The accuracy of synoptic scale surface wind fields derived directly from wind observations suffers from two major drawbacks: a paucity of observations, and the high variability of the small scale wind field. The small number

of observations usually available in a typical mid-ocean region over a three-or-four-day period are very often grouped together in a small section of the region, often along major shipping lanes or along the track of a single ship. In addition, major portions of the open ocean lack any reports of wind conditions for weeks at a time. As a result, the few reports available must necessarily be used to describe large areas when estimating the synoptic scale wind field. Verploegh (1967) found, however, that simultaneous wind speed observations from ships less than sixty miles apart in "synoptically homogeneous areas" differed significantly. His analysis indicated the correlation coefficient between such observations was less than 0.7.

Because of such considerations, the second, indirect approach is generally used to estimate the synoptic scale surface wind field. This approach depends on the fact that the distribution of surface atmospheric pressure can be more accurately described than can the surface wind field from a limited number of observations, due to the lower variability in time and space of the surface atmospheric pressure field. An accurate estimate of the synoptic-scale surface wind field may be made by applying the geostrophic approximation to the surface atmospheric pressure field.

B. OBJECTIVES

Although the relation of the geostrophic to observed wind is a popular topic, this study is not intended to be a detailed examination of that relation. Rather, it is limited to an evaluation of one particular surface wind model used, in this study, to hindcast time series of surface winds over oceanic areas. The model is quasi-geostrophic, incorporating the effects of friction. It is one part of operational oceanographic models used at Fleet Numerical Weather Central and at Fleet Weather Central, Rota (Spain).[1]

As a result of this study, the ten-year average and linear trend of observed wind conditions at several points in the North Atlantic and North Pacific Oceans were determined and compared to those calculated from the model. The primary objective of the study was however, to determine the accuracy of the computed time series and to determine if calibration factors could be applied directly to them in order to increase their accuracy.

---

[1]The model was developed by the author while at Fleet Numerical Weather Central; most of the work of this study was carried out while the author was at the Environmental Prediction Research Facility.

II. APPROACH

A. THEORETICAL BACKGROUND

1. The Geostrophic Wind Equation

Geostrophic wind has been considered to be an acceptable estimate of the true surface wind in many studies of oceanography and air-sea interaction (Roden op. cit., Namias, 1963). Geostrophy assumes a balance between the pressure gradient force and the Coriolis force and ignores acceleration, friction, and vertical motion. This balance is given in equation (1):

$$\hat{V}_g = \hat{k} \times \frac{1}{\rho f} \nabla_H P \qquad (1)$$

where $\hat{V}_g$ = geostrophic wind vector

P = surface pressure

$\nabla_H = \frac{\partial}{\partial x} \hat{i} + \frac{\partial}{\partial y} \hat{j}$ (horizontal gradient operator)

$\times$ = vector product operator

$f = 2\omega \sin \phi$ (the Coriolis parameter)

ω = angular rotation of the earth

ϕ = latitude

ρ = air density

$\hat{k}$ = unit vertical vector

Although this approximation is widely used, its accuracy is limited by the required assumptions indicated above.

The true surface wind vector is the resultant of the geostrophic wind vector and an ageostrophic wind vector. The direction and magnitude of the ageostrophic wind vector determines the accuracy of the geostrophic approximation. Unfortunately the ageostrophic vector has been shown to vary significantly over the Northern Hemisphere (Roll, 1965; Carstensen, 1967; Brümmer, et al., 1974). Such variability makes the geostrophic wind hard to relate to the surface wind in studies on synoptic or larger scales.

The accuracy of the geostrophic approximation is also limited, in practical application, by the temporal variability of the surface pressure field. In practice, the geostrophic approximation is often applied to surface pressure distributions averaged over a month or more (Namias, op cit.). Such a procedure results in calculating the vector resultant of the geostrophic wind for the averaging period. Obviously, non-conservative phenomena which depend on the surface wind cannot be treated using such a resultant wind field. In the study of such phenomena, the resultant vector is assumed to represent the mean or steady-state wind prevailing over the averaging interval.

Whether or not the resultant wind is a good estimate of the mean wind depends on the variance of the wind vector over that interval. The mean wind speed, W_M, and the resultant wind speed, W_R are given below in terms of components:

$$W_M = \frac{\sum_{t=1}^{T} (U_t^2 + V_t^2)^{\frac{1}{2}}}{T} \qquad (2)$$

$$W_R = \left[\left(\sum_{t=1}^{T} \frac{U_t}{T} \right)^2 + \left(\sum_{t=1}^{T} \frac{V_t}{T} \right)^2 \right]^{\frac{1}{2}} \qquad (3)$$

where U_t, V_t are orthogonal components of the wind vector at time t for $1 \leq t \leq T$. (Averaging twelve hourly data over thirty days, we have $1 \leq t \leq 60$). The difference between W_M^2 and W_R^2 can be expressed in terms of the variance of each of the components, σ_u^2 and σ_v^2, and of the wind speed, σ_w^2;

$$W_M^2 - W_R^2 = \sigma_u^2 + \sigma_v^2 - \sigma_w^2 \qquad (4)$$

where $$\sigma_u^2 = \sum_{t=1}^{T} \frac{U_t^2}{T} - \left(\sum_{t=1}^{T} \frac{U_t}{T} \right)^2 \qquad (5)$$

and similarly for σ_v^2, and σ_w^2. As will be shown in Section III-A, the difference expressed in equation (4) results in a drastic under-estimate of wind speed when the resultant wind is used in place of the mean wind speed in problems involving the square of the wind speed.

2. The Surface Wind-Geostrophic Wind Relation

Although this is not a study of the general relation of the geostrophic wind to the surface wind, a few words regarding this relation are appropriate for background. As indicated, the surface wind vector can be resolved into

geostrophic and ageostrophic components. The ageostrophic component can be assumed to consist of a frictional component and an acceleration component (Brümmer, et al., op cit.).

The frictional component is generally accepted as the dominant ageostrophic component (Verploegh, op cit., Brümmer, et al., op cit.). Haltiner and Martin (1957) suggest that the frictional component is dependent on the stability of the surface layer of the atmosphere. Hasse (1974) has demonstrated that the dependence of the surface wind speed on the surface pressure gradient is an order of magnitude greater than its dependence on stability.

The effects of stability have not been explicitly incorporated into the model; to some degree however, they have been implicitly incorporated through the latitude dependence of terms in the various equations of the model. The major effects of stability are assumed to occur in the region between 45°N and 25°N. This implicit incorporation of stability is shown in the ratio of the surface wind speed to the geostrophic wind speed in Figure 1.

B. METHOD OF COMPUTING THE SURFACE WIND

The calculations were performed on the Fleet Numerical Weather Central (FNWC) 63x63 polar stereographic grid of the northern hemisphere (FNWC, 1974). On this square grid the equator is an inscribed circle, i.e., tangent to the grid

boundary. The grid mesh length at 60°N is 381 km and increases with increasing latitude. The data, although calculated on a polar stereographic grid, will be discussed relative to a Mercator grid.[2]

The components of the horizontal pressure gradient at a given grid point (i,j), were approximated to the second order by equation (6):

$$\frac{\partial P}{\partial X}(i,j) = \frac{MF(i,j)}{L} K_1\{P(i-2,j) - K_2[P(i-1,j) - P(i+1,j)] - P(i+2,j)\} \quad (6)$$

where K_1 = 1/12

K_2 = 8

L = 381 km (mesh length)

$MF(i,j) = \frac{1+SIN(60°)}{1+SIN(\emptyset)}$ = map factor of the grid at point (i,j)

$\emptyset$ = latitude of grid point (i,j),

and similarly for $\frac{\partial P}{\partial Y}(i,j)$. Using (1) with a constant air density of 1.22×10^{-3} gm cm^{-3}, the geostrophic wind vector

---

[2]Both Mercator and polar stereographic projections are conformal projections of the earth and as a result, angles are preserved when transformed from one to the other (Taylor, 1955).

at each point was found.[3] The magnitude of this vector (the geostrophic wind speed) was then reduced as a function of the latitude of the grid point according to (7):

$$\hat{V}_s(i,j) = A\,[B(\emptyset)]\,\hat{V}_g(i,j) \qquad (7)$$

where $\hat{V}_s(i,j)$ = surface wind speed at grid point (i,j)

$\hat{V}_g(i,j)$ = geostrophic wind speed at grid point (i,j)

$A = 0.93$ [4]

$$B(\emptyset) = \begin{cases} 0.65+0.2(\emptyset/25°); & \emptyset < 25° \\ 0.85 ; & 25° \leq \emptyset \leq 45° \\ 0.75+0.1\frac{(90°-\emptyset)}{45°}; & 45° < \emptyset \end{cases}$$

The resulting ratio of (V_s/V_g), which is strongly dependent on latitude, was suggested by data from Roll (op cit.) and Carstensen (op cit.). The value of (V_s/V_g) used in the model is plotted in Figure 1 along with values

---

[3]The sine function, SILA, used in the calculation of the Coriolis parameter for the geostrophic wind calculation and in the calculation of the deflection angle (equations 1 and 8) was modified below 35°N. This was done in an attempt to reduce the impact of this parameter in the calculation of equatorial winds. The modification was suggested by the subroutine SNLTSRX in the Fleet Numerical Weather Central program library.(FNWC, op cit.). The value of SILA south of 35°N is given by the tangent to the sine curve at 35°N, i.e., $SILA(\emptyset) = 0.0144(SIN^{-1}(\emptyset)) + 0.075$ for $\emptyset \leq 35°$.

[4]The factor A resulted from erroneously using 408 km for the grid mesh length in the model (D. Dale, FNWC, personal communication).

found by Roll and by Carstensen. Although Carstensen derived his relation from a much smaller data set than that in Roll's study, the major features of the latitude dependence are similar. The value of (V_s/V_g) used in the present model attempts to reproduce the first order dependence on latitude: i.e., the maximum in the mid-latitudes, sharply decreasing with decreasing latitude toward the equator and a more modest decrease with increasing latitude above 45°N.

After being reduced in speed, the surface wind vector is then rotated to the left of the geostrophic wind vector (toward low pressure). Together, deflection and reduction of the geostrophic wind vector simulate the effects of friction (Haltiner and Martin, op cit.). The deflection angle, α, was calculated from (8):

$$\alpha = K_1 (K_2 - K_3 V_s^2) / (1+\text{SIN } \emptyset) \qquad (8)$$

where $K_1 = 1.475$

$K_2 = 22.5$

$K_3 = 1.75 \times 10^{-2}$

V_s = surface wind speed, from (7) .

Figure 2 is a plot of α against latitude for several values of surface wind speed.

The dependence of α on the square of the surface wind speed strongly decreases the deflection angle associated with high surface wind speeds. This approach was based on the assumption that high winds (associated with well-defined

cyclones) generally show less cross-isobar flow than do the low winds associated with nearly flat surface pressure distributions. The assumed reduction in the deflection angle as wind speed increases could be caused by a slight reduction in the frictional drag experienced at higher values of surface wind speed. In this model, however, this reduction becomes significant only at relatively high wind speed. For example, at 20 m sec^{-1} the deflection angle is 75% of its value at 1 m sec^{-1}. At 30 m sec^{-1} the deflection angle has been reduced to 30% of the value at 1 m sec^{-1}.

As with the value of (V_s/V_g), the latitude dependence of α also was suggested by Roll and Carstensen. Figure 3 is a plot of the value of α against latitude as found by Roll, by Carstensen, and as used in this model. The values of α from the model are those for surface wind speeds of 5 and 15 m sec^{-1}. Less than 15% of the reported wind speeds in this study were outside this range. As in the case of the reduction factor, the expression for α attempted to reproduce the major features of the latitude dependence shown by both Roll's and Carstensen's data.

C. DATA GENERATION

1. Input Data for the Model

The model was used to calculate a ten-year time series of the surface winds at twelve hour intervals at grid points near international Ocean Stations. The input for the model consisted of surface pressure fields on the FNWC grid.

All the available surface pressure analyses for synoptic periods of 0000 GMT and 1200 GMT were used for the ten-year period from 0000 GMT 1 January 1960 to 1200 GMT 31 December 1969. However, not all the analyses for this period were available and this required some conditioning of the output data which will be discussed in Section II-D.

The number of surface pressure analyses used for each month in the ten-year period are shown in Table I. In general, the analyses were fairly evenly distributed over the twelve months. The month of April had the poorest representation with 488 (81%) of the 600 possible analyses used, while November was the best represented with 534 (89%) of the 600 possible analyses. Most of the missing data were concentrated in the period from April 1960 through June 1962. Within this period only one analysis per day was available. As a result, only 365 (50%) of the 730 possible analyses were used for 1961. The best-represented year was 1967 for which 728 (99.7%) of the 730 possible analyses were available. The missing analyses totaled 1098 (15%) of the 7306 possible in the ten-year interval.

According to Bakun (1973), who used the same set of surface pressure analyses to calculate coastal upwelling indices, the analyses between January 1960 and July 1962 were from the National Climatic Center at Asheville, North Carolina. The analyses from July 1962 through December 1969 were produced by objective computer analyses at FNWC.

2. The Observational Data

The observed wind data were taken at six international Ocean Stations (OS). These were the only continuous time series of observed wind speed and direction available for the ten years of this study. As these data were assumed to be of high quality, no attempt was made to determine their accuracy other than gross error checking as described in Section II-D. The observations were thus used as the standard against which the calculated wind records were verified.

The observed wind speed and direction were extracted from the Surface Marine Observation Tape Family 11 from the National Weather Record Center for the following Ocean Stations: BRAVO (OSB), DELTA (OSD), JULIET (OSJ), PAPA (OSP), VICTOR (OSV), and NOVEMBER (OSN).[5] Table II indicates the position of each OS, the position of the computational grid points, and the distance between each OS and its corresponding grid point.

3. Data Used in Analysis

Both the observed and computed data were transformed to zonal (East-West) and meridional (North-South) components. The resulting set of three time series for each OS and each grid point (a total of 39) consisted of the values of zonal

---

[5]All the Ocean Station records with the exception of NOVEMBER (OSN) were compared to computational time series from a single grid point near their location. Time series were calculated at two grid points bracketing OSN in order to estimate the variability of the computed wind over a single grid mesh length. These computation grid points will be referred to, henceforth, as N1C and N2C.

and meridional components and the wind speed at 0000 GMT and 1200 GMT for the ten-year period from 1 January 1960 to 31 December 1969. It should be noted here that a negative zonal value indicates a wind from the West and a negative meridional value indicates a wind from the South.

D. DATA CONDITIONING

1. Gaps and Gross Errors

A check for gross errors was performed following extraction and transformation of the observed and computed wind vectors. A wind speed of 50 m sec^{-1} was selected as the maximum allowable value; this established a gross error criterion in order to eliminate only those errors caused by hardware failure such as tape parity. No wind speed values in excess of 50 m sec^{-1} were found in either the computed or observed data.

After gross error checking was completed, ensemble analysis was performed on the observed and computed time series. Following that, the gaps in the records were removed. The computed records differed markedly from the observational data in both the number and length of gaps. For the eighteen observational records, the number of single point gaps per record averaged about 200, while about 300 points per record were missing in gaps of two or more consecutive points. Only about 150 points per record were missing from the computed time series in the form of multiple point gaps. However, for

these computed records there were about 950 single point gaps, due primarily to missing pressure analyses within the period of April 1960 through June 1962.

Because of the high proportion of single missing data points in the calculated record, a single missing value was replaced by linear interpolation between the preceding and following value. For gaps consisting of two or more data points, the missing data were replaced by the time series average. This procedure was suggested as a means of filling gaps while not introducing spurious data into the records which would be subjected to subsequent spectral analysis.[6]

2. Filtering

Filtering was done on the computed and observed records in order to allow comparison of records with nearly equal data content. Because of the substantial missing data in the high frequency part of the computed record (due to single point gaps) and because of the stated interest in large scale phenomena, a low-pass filter was applied to each of the computed and observed time series after the gaps were

---

[6]E. Thornton, Dept. of Oceanography, Naval Postgraduate School, personal communication.

removed. A five-point binomial filter indicated in equation (9) was used.[7]

$$Y(t) = \sum_{i=-2}^{2} a_i \, X(t+i\Delta t) \qquad (9)$$

where $Y(t)$ = filtered value at time t

a_i = binomial coefficient (0.38, 0.25, 0.06, for $i = 0, \pm 1, \pm 2$)

$X(t+i\Delta t)$ = unfiltered value of the time series at time $t+i\Delta t$

Δt = sample interval (0.5 days)

Figure 4 shows the effect of applying this filter to a typical segment of one of the computed time series. The amplitude of the residual series (unfiltered minus filtered) is approximately the same amplitude as the filtered series, indicating that approximately 50% of the variance of the unfiltered series was removed by filtering. This estimate of 50% was confirmed by a comparison of the filtered and unfiltered record variance (not shown). Before any filtering or gap removal was done, however, the observed and computed records were analyzed as ensembles in order to determine the relation between them.

---

[7] Such a filter has a frequency response, $R(f)$, at frequency f

$$R(f) = \cos^4 (\pi f \Delta t) \qquad (10)$$

(Panofsky and Brier, 1958).

III. RESULTS

A. ENSEMBLE ANALYSIS

In this section the ensembles of the observed and computed data are compared. The term ensemble is taken to mean the set of values which constitute a given time series of the variable in question. Due to the length of the records (ten years), significant questions about short-term accuracy of the model cannot be treated by ensemble analysis. The problem of short-term accuracy is investigated through spectral analysis as reported in Section III-B.

1. Central Moments

Both the observed and computed data were considered to have come from specific probability densities. While these probability densities were not explicitly defined in this study, they were described by determination of their central moments. The general form of the central moment of a given probability density is given by equation (11).

$$\mu_R = \sum_{i=1}^{N} \frac{(x_i-\mu)^R}{N} \qquad (11)$$

where μ_R = R^{th} central moment

x_i = i^{th} value of the variable X

N = total number of values of X in the ensemble

$\mu = \sum_{i=1}^{N} x_i/N$

= mean value of the ensemble

In practice, the third and fourth moments are normalized by the third and fourth powers of σ ($\sigma = \mu_2$), the standard deviation of the ensemble (Tennekes and Lumley, 1972). In this study the first moment is taken to be the mean rather than zero as in equation (11).

The criterion used to estimate the accuracy of the computed data - the "figure of merit" - was the ratio of a central moment of the computed record to that of the observed record. This simple criterion was intended to show only two things: the percentage of a given observed statistic present in the corresponding computed record; and those statistics which differed in sign between computed and observed records (resulting in a negative figure of merit).

As the computed data were compared to observations at six[8] OS, the average figure of merit for the model was taken to be the average of the figures of merit for each OS. An average was found also for the three OS in the Pacific and for the three in the Atlantic.

a. Wind Speed

The values of the central moments and their figures of merit for the observed and computed wind speed are

---

[8]The two computed records, NC1 and NC2, were compared to the observational record at OSN. In order not to overemphasize these data when considering averages, the average of the figures of merit of NC2 and NC1 was used as the figure of merit at OSN when calculating the overall average figure of merit or the average of the figures of merit in the Pacific.

tabulated in Table III and are plotted against latitude in Figure 5. The average computed wind speed (first moment) varied between 95% and 91% of the average wind speed observed at the six OS. Over the latitude range of the OS (30°N to 56.5°N), the average observed wind speed decreased from a maximum of 10.6 m sec^{-1} in the Westerlies (OSP) to 6.6 m sec^{-1} in the North East Trades (OSN) for the ten years between 1960 and 1969. The average figure of merit for the mean computed wind speed is 0.92. This figure is 0.91 in the Pacific and 0.93 in the Atlantic.

It is worth noting again here that we are dealing with an average wind speed and not a resultant wind speed. The resultant wind speed can be determined by combining the average zonal and meridional components by vector addition. The average wind speed was determined from the wind speed at each interval in the ten year time series.

The variance (second moment) of the wind speed decreased from approximately 28 m^2 sec^{-2} in the latitudes of the Westerlies to approximately 10 m^2 sec^{-2} in the latitudes of the Trades - a latitude dependence similar to that of the average wind speed. The average figure of merit for the variance is 1.07. Only at OSB is the figure of merit (0.89) less than unity. The maximum (1.24) is shared by OSJ and OSN (NC2). When comparing the variances of the computed and observed records by means of the F test it becomes apparent that any figure of merit for the variance which is not equal

to unity is statistically significant at the 1% level due to the very large (>6000) number of degrees of freedom for each ensemble (Freund, 1962). That is, the probability that the computed and observed ensembles come from the same probability density is less than 0.01. Relating these statistically significant differences in the observed and computed records to to physical causes is, for the most part, beyond the scope of this study. However, the location of the grid point NC2 (at 32N) at the northern boundary of the North East Trades appears associated with the high figure of merit at this location. Seckel (op cit.) suggested the wind speed is much more variable at 32N (NC2) than it is in the Trades (at OSN), and thus a figure of merit for wind speed variance greater than 1.0 is to be expected between these records. This suggests that the model can resolve significant changes in the variability of the wind field which occur on a scale of one grid-mesh length.

The standard deviation (square root of the variance) can be used to estimate an upper bound on the average fluctuation of the wind speed from the ten-year mean. According to Chebyshev's Inequality, the probability that the wind speed will differ from the average by more than 1.414 standard deviations is less than 0.50 (Freund, op cit.). The value of 1.414 σ in the Westerlies was about 7 m sec^{-1}. This value is considerably greater than the diurnal range of the

wind speed in the open ocean reported by Roll (op cit.). Thus, most of the variance in the wind speed observed at OS over the ten-year period was due to variations of a period longer than twelve hours. The 50% reduction in the variance due to filtering as indicated in Section II-D-2 suggests that 50% of the variance is due to wind speed fluctuations of a period greater than two days.

The third moment (skewness) of the computed wind speed is higher than that of the reported wind speeds at all the OS. The average figure of merit for all the locations is 1.30. This high value represents a tendency of the computed wind speed to exceed reported wind speed significantly in cases of high wind. Of the locations studied, this tendency is most pronounced in the Pacific Trades. The fact that the average figure of merit was greater than one for the skewness and less than one for the average of the wind speed suggests that the overestimated high wind speeds in the computed record were more than compensated by more numerous underestimations of low wind speeds. The omission of the effects of curvature, i.e., the acceleration of the wind due to the centrifugal force, in the geostrophic equation was suggested as the cause of this effect.[9]

---

[9]R. Elsberry, Dept. of Meteorology, Naval Postgraduate School, personal communication.

The exaggeration of both extremely low and high wind speeds is also suggested by the fourth moment (kurtosis) which indicates the amount of extreme data in the ensemble, i.e., the number of data points in the ensemble which are far from the mean. The figure of merit for kurtosis is highest for the Pacific in the transition from Westerlies to Trades (OSV and OSN-NC2). As can be seen in Figure 5, the value of the kurtosis of the wind speed increases dramatically in the Trades. However, this increase is an artifact of the normalization by the fourth power of the standard deviation, which is much smaller in the Trades than in the Westerlies, and does not indicate that very strong winds occur more frequently in the Trades than in the Westerlies.

b. Zonal Component

The first four moments for the zonal component of the wind vector are shown plotted against latitude in Figure 6. Their values and figures of merit are tabulated in Table IV. The latitude dependence of the first moment (average or resultant) of the observed and computed zonal components is similar. The difference between the first moments of the observed and computed zonal components is greatest at OSP (0.85 m sec^{-1}). While the average figure of merit of the first moment is 1.0, the model is more accurate in the Atlantic than in the Pacific Ocean. In the Pacific the figure of merit ranges from 0.43 to 1.45 and averages 1.01. In the Atlantic the range was smaller, from 0.89 to 1.05, and the figure of merit averages 0.98.

This disparity between Atlantic and Pacific is evident also when comparing the variance (or second moment) of the observed zonal component to that of the computed zonal component. The figure of merit ranges between 0.83 and 0.95 in the Atlantic Ocean and between 0.78 and 1.02 in the Pacific. Overall, it averages 0.88, indicating that the model reproduced about 88% of the variance of the zonal wind. The relatively poor accuracy of the model at OSP as shown in Figure 6 is unexplained; however, the poor agreement between OSN and grid point NC2 is probably due to the transition to the Trades as previously suggested.

The skewness showed the poorest agreement of all the moments calculated for the computed and observed zonal components. The model consistently underestimated this parameter; the figure of merit averaged only 0.63. The signs of the computed and observed skewnesses differed at OSJ; however, the values at this point were so near zero that the difference is insignificant.

The kurtosis (fourth moment) of the computed zonal component was consistently higher than that of the observed zonal component. The average figure of merit was 1.11, and was nearly equal in both the Atlantic and Pacific Oceans.

c. Meridional Component

The first four moments of the probability density of the computed and observed meridional components are tabulated in Table V and are plotted against latitude in Figure 7.

The figure of merit for the mean of the meridional component, averaged for all locations, was 1.22 and was nearly equal in the Pacific and the Atlantic Oceans. The individual figures of merit of the means suggest that the computed meridional component has a bias of 0.3 to 0.9 m sec^{-1}. This bias is a fictitious (computed) component from the south, which reduced the average computed meridional component at those stations where the resultant direction was from the north (OSB and OSN); and it increased the meridional component at those stations where the resultant direction was from the south. Such a consistent bias suggests that a fictitious east-west gradient (higher pressure to the east) in the surface pressure analyses may occur over both the Pacific and Atlantic Oceans.

The variance of the observed and computed meridional components showed only slightly better agreement than was the case for the zonal component. Averaged over the locations studied, the model reproduced 92% of the variance of the observed meridional component. Again, OSN (NC2) showed the highest figure of merit due to the effects of the transition to the Trades.

The skewness of both the observed and computed values was nearly zero at all locations north of the Trades. This indicates that, relative to the average meridional component, the strong positive (northerly) and negative (southerly) fluctuations were equally distributed. The

negative value of the skewness at OSN indicates that the southerly (relative to the mean) extremes predominated. Because the skewness was so near zero for all stations north of the Trades, figures of merit at these locations have little meaning. In the Trades, the model overestimated the skewness by up to 98%. This very high figure of merit is in marked contrast to that for the skewness of the zonal component (Table IV). This discrepancy suggests that in the Trades, extreme values in the calculated record of meridional components are not always matched in the observed record.

The value of the kurtosis (fourth moment) of the meridional component was slightly overestimated by the model. The figure of merit averaged 1.19, and the averages for the Atlantic and Pacific Oceans were identical.

The values of the skewness and kurtosis of the meridional component north of the Trades, approximately 0 and 3.0 respectively, suggest that the values of the meridional component exhibit the well known Gaussian distribution in this area.

Of the four central moments discussed above, perhaps the most important for oceanographic purposes is the variance. This parameter is a measure of the kinetic energy of the wind, and is directly related to the frictional coupling of the ocean and atmosphere.

On the average, for the locations studied, the model reproduced about 90% of the variance in each of the components of the wind vector and overestimated the variance

of the wind speed by 7%. In none of the cases was the error greater than 25%. The consistent overestimation of the variance at NC2 as compared to NC1 indicates that features such as the transition from the Trades to Westerlies can be resolved within one mesh length of the computation grid.

The difference, shown in equation 4, between the square of the mean wind speed (derived from individual pressure analyses as in this study) and the square of the resultant wind speed (derived from monthly mean pressure analyses) is often neglected in studies of large scale air-sea interaction (Namias, op cit.). As can be seen from Tables III through V, this difference as observed at OSP is 92.5 m^2 sec^{-2}. The resultant wind squared is only 20.7 m^2 sec^{-2}. In this case the resultant square is less than 20% of the mean squared (112.2 m^2 sec^{-2}).

The difference between the ten-year mean and ten-year resultant is of course larger than the corresponding difference over a month due to the longer period (seasonal and year-to-year) variation. However, this example does show that the difference between the square of the mean and the square of the resultant can not be considered insignificant when dealing with the energetics of large scale air-sea interaction.

2. Ten-Year Trend

The estimation of a time series of wind conditions using pressure analyses from different sources raises a problem cited by Bakun (op cit.). That is, any long-term

trend in the wind record may be due to different methods of analyzing the pressure distribution in successive time intervals. For example, if improved analysis techniques or more numerous pressure reports allowed better resolution of tight pressure gradients there could be a fictitious increase in the wind speed derived from the improved pressure analyses. Obviously, such a fictitious increase should not be reflected in the long-term trend of observed wind speeds.

In order to investigate this possibility, the ten-year changes in the observed and computed wind speeds and components were calculated using equation (12) (Bendat and Persol, 1971).

$$\hat{u}(t) = b_o + b_1 t \tag{12}$$

where $\hat{u}(t)$ = value of trend line at time t,[10] and

$$b_o = \frac{2(2N+1)\sum_{n=1}^{N} u_n - 6\sum_{n=1}^{N} nu_n}{N(N-1)} \tag{13}$$

$$b_1 = \frac{12\sum_{n=1}^{N} nu_n - 6(N+1)\sum_{n=1}^{N} u_n}{h\,N(N-1)(N+1)} \tag{14}$$

---

[10] The sample interval, h, in equation (14) is assumed to be equal to 1. However, the gaps in the record were not filled prior to the determination of the ten-year trend. Because the vast majority of the gaps consisted of a single missing data point, this should have little impact in the determination of the ten-year change.

u_n = n^{th} value of the ensemble

N = total number of values in the ensemble.

The change over the ten-year period, Δ, is given by equation (15):

$$\Delta = b_1 N \ . \qquad (15)$$

The values of Δ for the wind speed and each of the components are shown plotted against latitude in Figure 8.

In the Westerlies the reported wind speed has decreased over the ten years between 1960 and 1970. In the Trades (OSN) it has increased very slightly. The decrease appears to be most pronounced in the Atlantic Ocean with a maximum decrease of 1.16 m sec^{-1} at OSJ. For the other locations the ten-year change was less than 0.6 m sec^{-1}. Computed wind speeds showed changes similar to those observed at all locations with the exception of OSP, where the slight increase of the computed speed (in opposition to the observed decrease) is unexplained.

With the exception of OSJ and OSN the values of the observed zonal components show a general increase over the ten years of the study. It should be noted that, due to the negative sign of the prevailing zonal component in the Westerlies and the positive sign in the Trades, this represents a decrease in the prevailing zonal components at all the locations except at OSJ.

At OSJ the observed increase in the prevailing zonal component was not accompanied by an increase in the prevailing meridional component. In fact, the prevailing observed meridional components decreased at all locations, with the exception of OSD.

Although there are noticeable differences between the trends of the computed and observed series, i.e., OSV (zonal), OSD (meridional) and OSP (speed), the similarity in latitude dependence and magnitude between observed and computed records suggests that the trends in the computed series are largely controlled by processes controlling the trend of the observed series, and are not due to artificial changes in the pressure data.

3. Correlation and Regression Analysis

This section deals with the linear correlation and non-linear regression analyses carried out on the ensembles of paired (computed and observed) data. Non-linear (parabolic) regression was done in order to determine the non-linearity of the relation between the computed wind data and those observed at the OS.

The linear correlation coefficient, R, is found using equation (16):

$$R = \frac{\sum_{n=1}^{N} (x_n - \bar{x})\,(y_n - \bar{y})}{\left[\sum_{n=1}^{N} (x_n - \bar{x})^2 \sum_{n=1}^{N} (y_n - \bar{y})^2\right]^{\frac{1}{2}}} \qquad (16)$$

where x_n = computed value

y_n = observed value

$$\bar{x} = \sum_{n=1}^{N} \left(\frac{x_n}{N}\right)$$

$$\bar{y} = \sum_{n=1}^{N} \left(\frac{y_n}{N}\right)$$

The value of R^2 is a measure of the dependence of the variability of one variable on the variability of the other through linear coupling (Panofsky and Brier, op cit.). Table VI indicates the values of R and R^2 for the wind speed and components, and the number of paired values upon which the correlation is based. In all cases, the correlation between computed and observed values of the components exceeds that between computed and observed speed. Averaged over the six OS, the model explained 65% of the variance in each of the components and 42% of the variance in the wind speed.

The lower correlation for wind speed can be attributed to the combined effect of errors in both the zonal and meridional components. If the computed wind vector is $\hat{W}_c$, then

$$\hat{W}_c = Z_c \hat{i} + M_c \hat{j} \qquad (17)$$

where Z_c and M_c are the computed zonal and meridional components and $\hat{i}$, $\hat{j}$ are unit vectors in zonal and meridional directions. If we also define the wind error vector $\hat{W}_e$ as:

$$\hat{W}_e = \hat{W}_c - \hat{W}_o \ , \tag{18}$$

where $\hat{W}_o$ is the observed wind vector

$$\hat{W}_o = Z_o\hat{i} + M_o\hat{j} \ , \tag{19}$$

we have, in terms of components,

$$\hat{W}_e = (Z_c - Z_o)\ \hat{i} + (M_c - M_o)\ \hat{j}; \tag{20}$$

and the wind speed error (magnitude of the error vector) is given by

$$W_e = \{(Z_c - Z_o)^2 + (M_c - M_o)^2\}^{\frac{1}{2}} \tag{21}$$

Thus, the error (and resulting lack of correlation) in the wind speeds should always be greater than or equal to the error (and lack of correlation) in the components; i.e., the correlation coefficient for the wind speed should always be less than that for either of the components.

On the average, the computed data correlated best with observations for the zonal components. In the Atlantic Ocean 67% of the observed variance in the zonal component was explained by the model. However, the meridional component showed higher correlation than the zonal component for five of the seven series.

In addition to linear correlation, non-linear regression between the computed and observed records were also determined. The regression equations are given below:

$$Y = A_o + A_1 X + A_2 X^2 \tag{22}$$

$$X = B_o + B_1 Y + B_2 Y^2 \tag{23}$$

where Y = computed value

X = observed value

The coefficients were found by solving the following set of simultaneous equations (24a - 24c) (Spiegel, 1961) for the computed data as a function of the observations, and solving the inverse set (replacing Y by X and solving for B_o, B_1 and B_2) for the observations as a function of the computed data.

$$\Sigma Y = A_o N + A_1 \Sigma X + A_2 \Sigma X^2 \tag{24a}$$

$$\Sigma XY = A_o \Sigma X + A_1 \Sigma X^2 + A_2 \Sigma X^3 \tag{24b}$$

$$\Sigma X^2 Y = A_o \Sigma X^2 + A_1 \Sigma X^3 + A_2 \Sigma X^4 \tag{24c}$$

Table VII lists the coefficients A_o, A_1, and A_2 for equation (22). Table VIII gives the coefficients for the inverse equation (23). The values of N, the number of paired data values in each series, are found in Table VI.

Comparing A_1 to A_2 and B_1 to B_2 indicates that an essentially linear relation exists between the computed records and observed records. The non-linear coefficients, A_2 and B_2, are two orders of magnitude less than A_1 and B_1 for all series except for the meridional component at OSN. At this location the non-linear term was only one order of magnitude less than the linear term.

Figures 9 and 10 are plots of the two regression equations for wind speed at OSJ and OSN (NC2). These locations showed the highest and lowest correlation between observed and computed wind speed. The separation of the two regression curves is due to the scatter of the computed and observed wind speed data being compared, as shown in Figures 11 and 12 (together with Table IX). The scatter of the data is at least partially due to neglecting some of the significant physics in the model, i.e., stability, and the curvature of the isobars in the pressure analyses. The area where the regression lines converge (the area of least scatter) is the area of best fit of the model. For OSJ this region is centered around 11 m sec^{-1}; for OSN it centers around 7 m sec^{-1}. In all cases this region of best fit is near the mean value of the series.

If the relation of the computed parameter to the observed parameter changes with time, then no single time-independent equation can express this relation. For the purposes of describing the relative accuracy of the model at various locations, however, the relation between the

observed and computed data is assumed to be shown by a single "true" regression line. The "true" regression line is defined as that line bisecting the distance between the two regression curves X = f(Y) and Y = f(X). This distance is measured perpendicular to the X=Y line. The "true" regression lines were found by graphical means for the wind speed at OSJ and OSN and are plotted in Figures 9 and 10.

These figures indicate that a consistent feature of the model, overestimation of high observed wind speeds and underestimation of low values, is most pronounced in the low latitudes (OSN) where observed wind speeds below about 11 m sec^{-1} are underestimated. This underestimation occurs to a lesser degree at OSJ up to wind speeds of about 14 m sec^{-1}. The scatter cannot be reduced by applying correction factors (deduced from the regression analysis) to the output of the model; however, taking average values of the model output over periods longer than 12 hours will provide a more accurate time series (at the expense of reduced time resolution). This is a result of the elimination of the extreme values in the time series by the averaging process. As the averaging interval increases, the mean over that interval approaches the mean of the time series in question. This set of means will then exhibit less scatter than the original series as they will be in the neighborhood surrounding the point where the two regression lines [X=f(Y) and Y=f(X)] intersect the X=Y line.

4. Error Analysis

Two sources of error, in addition to the neglected physics, are separation distance and the effects of friction in low latitudes. Investigation of the accuracy of the surface pressure distribution from which the wind records were calculated, a third possible error source, is beyond the scope of this thesis.

a. Separation Distance

The computational grid points do not exactly coincide with the locations of the OS where the observations were made. The distance between the grid point and OS is defined as the separation distance. The effect of separation distance on the mean error, i.e., the difference between the mean of the observed record and that of the computed record, is shown plotted against separation distance in Figure 13.

The mean error of the wind speed shows no relation to separation distance. However, such a relation is recognizable for the components of the wind vector. The meridional component mean error shows a slight increase with increasing separation distance. Although there is considerable scatter, there does not seem to be any significant difference between Atlantic and Pacific OS in this regard.

This is obviously not the case for the zonal component however. The Atlantic OS show little mean error in the zonal component. At Pacific OS, however, a rather pronounced dependence on separation distance is evident.

This dependence suggests the following:

(1) The ten-year average of the north-south pressure gradient (from which the zonal wind is derived) is more accurately described in the North Atlantic than in the North Pacific Ocean.

(2) The accuracy of this average gradient within 200 km of OS in the Pacific is, in part, dependent on the distance from the OS.

In addition to the effect of separation distance on mean error, its effect on the correlation between computed and observed records was also investigated. The results, shown in Figure 14, indicate no correlation coefficient dependence on separation distance comparable to that for mean error.

b. Friction in Low Latitudes

Low latitude wind fields play a very important part in large scale air-sea interaction (Berjknes, 1969; White and Walker, 1973). However, the wind fields in this region are typically difficult to model because they are strongly ageostrophic. As no data comparable to OS observations were available from low latitudes for direct verification, this section is included as an attempt to evaluate the accuracy of the model in this region.

In a recent study, Brümmer, et al. (1974) summarized data suggesting that the strong ageostrophic component of the surface wind vector in low latitudes was due to the effects of friction. These effects resulted in a reduced ratio, C, of surface wind speed to geostrophic wind speed and an increase in the deflection angle, α. Table X lists the values of C and α as reported by Brümmer, et al., and those used in the model at corresponding latitudes. (The values of α as used in the model are for surface wind speeds of 2.5 m sec^{-1}.) Although the values of C, as tabulated by Brümmer, et al., show no latitude dependence similar to those used in the model, they agree fairly well in magnitude. The value of α used in the model were close to those tabulated by Brümmer , et al., with the exception of α at 2°N.

At this latitude the values of α and C as used in the model could result in an error in the orientation of the surface wind vector, and corresponding errors in the components. For example, in the case of pure zonal flow, an error of 30° in α would reduce the zonal component to 0.866 of its original value and introduce a fictitious meridional component equal to 0.5 of the original zonal value. Such a fictitious meridional component in the computed record could lead to erroneous conclusions concerning the correlation of zonal and meridional wind stress anomalies. However, for the latitudes north of about 5°N, the parameterization of α and C appear to be reasonable.

B. SPECTRAL ANALYSIS

The method of analysis described in the preceding section allowed comparison of computed and observed values only as ensembles. This section describes the results of a comparison of frequency components constituting the observed and computed time series using spectral analysis. No attempt will be made to discuss the atmospheric dynamics implied by the spectra.

1. Autocorrelation

The autocorrelation function is the basis of spectral analysis. It describes the relative amplitude of the different frequency components present in a given time series (Bendat, Peirsol, op cit). The autocorrelation $R_{XX}(\tau)$ can be defined as:

$$R_{XX}(\tau) = \lim_{T\to\infty} \frac{1}{T} \int_0^T \{X(t)x(t+\tau)\}\, dt \qquad (25)$$

where

τ = lag interval

T = total time of the record

t = time variable

For this study T consisted of the ten years from 1960 through 1969, corresponding to 7306 twelve hourly increments of t. The lag interval ranged between 0 and one year

(731 twelve-hour increments). Because of the gaps in the observed record and the filtering performed on the time series (see Section II-D), the spectral analysis data are presented only for frequencies greater than 0.5 cycles day^{-1}.

Table XI presents, at selected frequencies, the values of the autocorrelation function of the computed and observed time series at OSB and OSV. The frequency is determined by the lag interval τ, which is the period of the frequency component in question. The discussion of the autocorrelation function is intended to illustrate the nature of the periodicity of the observed time series and the differences between them. (The accuracy of the model at specific frequencies is best described by the phase and coherence functions discussed in Section II-B-3.) All of the computed series were expected to show autocorrelation higher than the observed data for short lags (0 to 48 hours) due to the averaging nature of the geostrophic approximation (Munk, 1960). This, however, was not the case at either OSB or OSV. However, because the data were heavily smoothed at these frequencies the differences may be masked. The values of $R_{xx}(\tau)$ for the observed and computed wind speed at OSB and OSV are shown plotted against lag time in Figures 15 and 16. The annual variation in wind speed is more pronounced at OSV than at OSB in spite of the fact that OSB is at a higher latitude. The reduced values of $R_{xx}(\tau)$ at annual and semi-annual frequencies at OSB can be attributed to a stronger

random component in the wind speed at these frequencies. (OSV perhaps is influenced by the Monsoon regime as suggested by Malkus, 1962.)

The nature of $R_{xx}(\tau)$ for the zonal component differs dramatically between OSB and OSV as shown by Figures 17 and 18. At OSB the zonal component is essentially random for lags longer than 4 days. This is not the case at OSV where annual variation is pronounced. The flattened minimum at OSV (Figure 18) indicates that the semi-annual periodicity (between 100 and 250 days) of the zonal component was reduced at this location by random fluctuations.

The meridional component at both OSB and OSV, Figures 19 and 20, show predominately random nature for lags greater than 4.0 days. However, Figures 19 and 20 show that the meridional component at OSB has a slightly more periodic nature than at OSV.

The computed series at both OSB and OSV show the same general features as do the corresponding observed records. In most cases even the minor details of $R_{xx}(\tau)$ for the observed record are also present in the $R_{xx}(\tau)$ for computed record. This suggests that the aperiodic as well as the periodic nature of the wind is accurately reproduced by the model.

2. Energy Density

For a given frequency, f, the energy density, $G_{xx}(f)$ can be expressed in terms of the autocorrelation function as follows:

$$G_{XX}(f) = 2 \int_{-\infty}^{\infty} R_{XX}(\tau)\, e^{-i2\pi f\tau}\, d\tau \qquad (26)$$

where $R_{XX}(\tau)$ = autocorrelation for lag τ. This relation is a Fourier transform from period space (τ) to frequency space (f). The area under a given segment of the energy density curve is proportional to the variance of the time series in that frequency range.

The energy density at frequencies equivalent to the lags (periods) listed in Table XI in the preceding section are listed in Table XII. A general underestimation of the energy by the model is indicated by this table and by the reduced value of the variance of the computed component records as indicated in Section (III-A). Most of the "missing" variance in the computed records occurs at frequencies less than 0.1432 cycles day^{-1} (periods greater than 1 week). The dependence of the energy density on frequency for the computed and observed records is shown in the upper diagrams of Figures 21 through 26. It should be noted that the plot of the logarithm of the energy density tends to overenhance the absolute differences at high frequencies and to mask them at low frequencies.[11]

---

[11] The scale of the spectral energy-density plot varies from figure to figure as a result of attempting to maximize the resolution of data, which varied significantly from plot to plot.

However, the plots indicate that the model's accuracy is not significantly dependent on frequency and that the geographical differences of the observed wind spectra are accurately reproduced in the computed wind spectra. Geographical differences are especially evident in the spectra of the components; this indicates that for purposes of large scale numerical modeling of sea-air interaction, uniform, zonal-averaged wind fields cannot be considered realistic.

3. Coherence and Phase

Coherence is a measure of the correlation between two time series at a given frequency; as such, it is the best estimator of the accuracy of the model. It can be defined in terms of the energy-density spectra of each of the two-time series of two variables, x and y, and their cross spectra. The equation for coherence, γ_{xy}, is given in equation (27).

$$\gamma_{xy}(f) = \frac{\{G_{xy}(f)\}^2}{G_{xx}(f)\, G_{yy}(f)} , \qquad (27)$$

where $G_{xx}(f)$ and $G_{yy}(f)$ are the energy densities of the computed and observed time series as described in the previous section. The cross-spectral density function, $G_{xy}(f)$, is defined in terms of the cross correlation function between the variables x and y, $R_{xy}(\tau)$ (Bendat and Peirsol, op cit.).

$$G_{xy}(f) = 2 \int_{-\infty}^{\infty} R_{xy}(\tau) e^{-i2\pi f\tau}\, d\tau \qquad (28)$$

where the cross correlation function is given by:

$$R_{xy}(\tau) = \lim_{T\to\infty} \int_0^T x(t)y(t+\tau)dt \qquad (29)$$

If $\gamma_{xy}(f) = 1$, the records are perfectly correlated at frequency f; for $\gamma_{xy}(f) = 0$, no relation exists between x and y at that frequency.

Another estimator of the accuracy of the model derived from the cross-spectral density function is the cross-spectral phase angle, $\phi_{xy}(f)$. This function measures, at frequency f, the average angular difference between the time series of x and y, and is defined in terms of the real and imaginary parts of the cross-spectral energy-density function:

$$\phi_{xy}(f) = \tan^{-1} [Q_{xy}(f) / C_{xy}(f)] \qquad (30)$$

where $Q_{xy}(f)$, the imaginary part of $G_{xy}(f)$, is called the quadrature spectral-density function; and $C_{xy}(f)$, the real part of $G_{xy}(f)$, is called the coincident spectral-density function. $C_{xy}(f)$ and $\phi_{xy}(f)$ can be defined as follows:

$$C_{xy}(f) = \tfrac{1}{2} \{G_{xy}(f) + G_{yx}(f)\} \qquad (31)$$

$$Q_{xy}(f) = \frac{i}{2} \{G_{xy}(f) - G_{yx}(f)\} \qquad (32)$$

For this study a positive phase angle indicates the computed record lags the observed record in time. For example, a cross-spectral phase angle equal to +9° at a frequency of 0.1 cycles day^{-1} indicates that the component of computed record at this frequency lags the observed record by 0.25 days or 6 hours.

The values of the coherence and phase (cross-spectral phase angle) at OSB and OSV for the frequencies of interest are tabulated in Tables XIII and XIV. In Figures 21 through 26 the coherence and phase are plotted in the lower two diagrams. At both OSB and OSV there is a gradual increase in coherence with decreasing frequency. As suggested in Section III-A-3, the coherence between computed and observed wind speed is lower than is the coherence between the observed and computed components. At OSB there is a constant increase in $\emptyset_{xy}(f)$ with increasing frequency. For the wind speed and the components of the wind vector this phase difference is approximately 45° at f=0.5 cycles day^{-1}, indicating the computed record lags the observed by about 6 hours.

For OSV there is no consistent phase difference between the observed and computed records similar to that at OSB; however, the coherence is similar to that for OSB, and approaches unity at periods of six months and a year.

The data presented in this section suggest that this model reproduces the major features of the observed energy density spectra of wind speed and orthogonal components for frequencies between 0.5 and 0.0027 cycles day^{-1} (periods of 12 hours to one year). It also suggests that spectra for the components of the wind vector cannot be deduced from the corresponding spectra of the wind speed.

IV. SUMMARY

A. ACCURACY OF THE MODEL

The results of this study suggest the following:

1. The relation between the computed and observed records of wind speed and components of the wind vector is essentially linear.

2. The model exaggerates both high and low values of wind speed and components and this exaggeration is most pronounced at low latitudes.

3. The accuracy of the model as shown by correlation with observations is slightly higher in the Atlantic compared to the Pacific Ocean; and it is higher in mid-latitudes than in either high or low latitudes.

4. The ten-year (1960-1969) trend of wind conditions between 29°N and 56.5°N is similar for both the computed records and the observed records; and observations indicate a slight reduction (~0.5 m sec^{-1}) in wind speed over the northern hemisphere between 35N and 50N.

5. The model explains between 30% and 70% of the variance of the parameters measured at 12-hour intervals.

6. There is a fictitious southerly component incorporated in the computed records at all grid points, possibly the result of a fictitious east-west gradient in the pressure analyses used.

7. The deflection angle between the surface wind and the geostrophic at latitudes between 0° and 5°N as used in the model is substantially less than the values thus far observed.

8. The accuracy of mean wind conditions derived from the model increases with the length of the averaging interval, as indicated by increasing coherence with longer period fluctuations.

B. POSSIBLE APPLICATIONS

The last conclusion points to a possible application of the model in addition to its current operational use. Monthly means of wind conditions derived from 12-hourly surface pressure analysis using the model should exhibit even greater accuracy than do the 12-hourly values. The mean wind parameters derived in this way would be true averages and not resultant wind parameters. A historical record of this nature should permit a more realistic quantitative approach to sea-air interaction studies than has been the case to date.

TABLE I

Monthly distribution of surface pressure analyses. The number of analyses used is in the numerator, and the denominator equals the number of twelve hour intervals in the month.

YR / MN	1960	1961	1962	1963	1964	1965	1966	1967	1968	1969	TOTAL
I	61/62	31/62	31/62	54/62	56/62	61/62	61/62	62/62	62/62	62/62	541/620
II	58/58	28/56	28/56	52/56	58/58	54/56	56/56	56/56	58/58	56/56	504/566
III	62/62	31/62	31/62	49/62	55/62	46/62	58/62	62/62	62/62	62/62	518/620
IV	30/60	30/60	30/60	49/60	54/60	57/60	60/60	60/60	58/60	60/60	488/600
V	31/62	31/62	31/62	56/62	54/62	50/62	61/62	62/62	62/62	62/62	500/620
VI	30/60	30/60	30/60	54/60	57/60	60/60	59/60	60/60	59/60	60/60	499/600
VII	31/62	31/62	53/62	53/62	61/62	61/62	61/62	62/62	61/62	62/62	536/620
VIII	31/62	31/62	41/62	59/62	62/62	62/62	62/62	60/62	62/62	59/62	529/620
IX	30/60	30/60	57/60	33/60	59/60	59/60	59/60	60/60	60/60	60/60	507/600
X	31/62	31/62	59/62	36/62	61/62	61/62	45/62	62/62	62/62	62/62	510/620
XI	30/60	30/60	58/60	58/60	59/60	60/60	60/60	60/60	59/60	60/60	534/600
XII	31/62	31/62	58/62	58/62	57/62	60/62	62/62	62/62	62/62	61/62	542/620
TOTAL	456/732	365/730	507/730	611/730	693/732	691/730	704/730	728/730	727/730	726/732	6208/7306

TABLE II

Positions of the Ocean Stations, computational grid points and the distance between them.

SERIES	SHIP POSITION		GRID POINT POSITION		SEPARATION
	LATITUDE	LONGITUDE	LATITUDE	LONGITUDE	DISTANCE (km)
BRAVO	56.50 N	51.00 W	56.36 N	48.00 W	187
JULIET	52.00 N	20.00 W	53.48 N	19.06 W	176
PAPA	50.00 N	145.00 W	50.58 N	143.44 W	128
DELTA	44.00 N	41.00 W	45.37 N	41.34 W	154
VICTOR	34.00 N	164.00 E	34.11 N	165.00 E	96
NOVEMBER 2	30.00 N	140.00 W	31.45 N	139.04 W	186
NOVEMBER 1	30.00 N	140.00 W	29.06 N	140.64 W	120

TABLE III

Central moments and figures of merit (FM) of the distribution of observed and computed (C) wind speeds for each Ocean Station.

SERIES	LAT. N	MEAN	FM	VARIANCE	FM	SKEWNESS	FM	KURTOSIS	FM
BRAVO	56.50	10.39		28.9		0.65		3.28	
BRAVO (C)	56.36	9.76	0.94	25.6	0.89	0.78	1.20	3.54	1.08
JULIET	52.00	10.31		22.8		0.62		3.73	
JULIET (C)	53.48	9.78	0.95	28.3	1.24	0.77	1.24	3.74	1.00
PAPA	50.00	10.59		26.6		0.57		3.34	
PAPA (C)	50.58	9.58	0.90	27.1	1.02	0.74	1.30	3.63	1.09
DELTA	44.00	10.29		28.6		0.84		4.06	
DELTA (C)	45.37	9.61	0.93	30.6	1.07	0.95	1.13	4.23	1.04
VICTOR	34.00	8.23		19.2		0.85		3.90	
VICTOR (C)	34.11	7.46	0.91	21.4	1.11	1.15	1.35	5.03	1.29
NOVEMBER	30.00	6.55		10.4		0.84		4.91	
NOVEMBER (2)	31.45	5.97	0.91	12.9	1.24	1.31	1.56	5.97	1.22
NOVEMBER (1)	29.06	5.99	0.91	10.8	1.04	1.03	1.21	5.00	1.02
PACIFIC			0.91		1.09		1.40		1.17
ATLANTIC			0.93		1.06		1.19		1.04
ALL			0.92		1.07		1.30		1.10

TABLE IV

Central moments and figures of merit (FM) of the distribution of observed and computed (C) zonal components for each Ocean Station.

SERIES	LAT. N	MEAN	FM	VARIANCE	FM	SKEWNESS	FM	KURTOSIS	FM
BRAVO	56.50	-1.25		72.6		0.29		3.11	
BRAVO (C)	56.36	-1.11	0.89	64.5	0.89	0.27	0.93	3.23	1.04
JULIET	52.00	-3.18		62.0		0.09		2.99	
JULIET (C)	53.48	-3.33	1.05	58.6	0.95	-0.01	-0.11	3.51	1.17
PAPA	50.00	-4.29		61.1		0.23		3.29	
PAPA (C)	50.58	-3.44	0.80	47.9	0.78	0.17	0.74	3.51	1.07
DELTA	44.00	-3.65		61.2		-0.10		3.44	
DELTA (C)	45.37	-3.67	1.01	50.6	0.83	-0.03	0.30	3.73	1.08
VICTOR	34.00	-1.27		42.5		-0.24		3.29	
VICTOR (C)	34.11	-1.85	1.45	36.9	0.87	-0.23	0.96	3.97	1.21
NOVEMBER	30.00	2.57		23.1		-0.62		4.24	
NOVEMBER (2)	31.45	1.12	0.43	23.5	1.02	-0.62	1.00	4.70	1.11
NOVEMBER (1)	29.06	2.91	1.13	19.1	0.83	-0.58	0.94	4.48	1.06
PACIFIC			1.01		0.86		0.89		1.12
ATLANTIC			0.98		0.89		0.37		1.09
ALL			1.00		0.88		0.63		1.11

TABLE V

Central moments and figures of merit (FM) of the distribution of observed and computed (C) meridional components for each Ocean Station.

SERIES	LAT. N	MEAN	FM	VARIANCE	FM	SKEWNESS	FM	KURTOSIS	FM
BRAVO	56.50	0.63		62.5		0.00		2.94	
BRAVO (C)	56.36	0.31	0.49	59.1	0.95	-0.12	...	3.39	1.15
JULIET	52.00	-1.22		55.5		0.07		2.68	
JULIET (C)	53.48	-2.16	1.77	49.7	0.90	0.09	1.29	3.27	1.22
PAPA	50.00	-1.52		57.0		0.11		3.11	
PAPA (C)	50.58	-2.26	1.49	54.1	0.95	0.05	0.45	3.49	1.12
DELTA	44.00	-1.19		58.7		0.03		3.08	
DELTA (C)	45.37	-1.70	1.43	55.9	0.95	0.03	1.00	3.74	1.21
VICTOR	34.00	-1.01		41.8		0.01		3.03	
VICTOR (C)	34.11	-1.53	1.51	34.4	0.82	-0.06	-6.00	3.77	1.24
NOVEMBER	30.00	0.55		23.3		-0.43		3.70	
NOVEMBER (2)	31.45	0.27	0.49	23.7	1.02	-0.70	1.63	4.16	1.12
NOVEMBER (1)	29.06	0.44	0.80	19.1	0.82	-0.85	1.98	4.89	1.32
PACIFIC			1.22		0.90		....		1.19
ATLANTIC			1.23		0.93		....		1.19
ALL			1.22		0.92		....		1.19

TABLE VI

Linear correlation coefficient (R) and coefficient of determination (R^2) between observed and computed time series for each Ocean Station.

SERIES	GRID PT. LAT. N	PAIRED VALUES	ZONAL		MERIDIONAL		SPEED	
			R	R^2	R	R^2	R	R^2
BRAVO	56.36	5941	.828	.686	.764	.584	.632	.399
JULIET	53.48	5829	.844	.712	.858	.736	.700	.490
PAPA	50.58	6051	.822	.676	.837	.701	.691	.477
DELTA	45.37	6002	.785	.616	.802	.643	.639	.408
VICTOR	34.11	5992	.798	.637	.800	.640	.662	.438
NOVEMBER 2	31.45	5890	.769	.591	.788	.621	.595	.354
NOVEMBER 1	29.06	5891	.761	.579	.759	.576	.540	.292
PACIFIC	38.31	5978	.795	.633	.804	.647	.640	.412
ATLANTIC	51.74	5924	.819	.671	.808	.654	.657	.432
ALL	45.02	5942	.807	.652	.806	.651	.648	.422

TABLE VII

Coefficients for regression of computed time series on observed time series for each Ocean Station.

SERIES	GRID PT. LAT. N	A_0			A_1			A_2 X 100		
		ZONAL	MERID.	SPEED	ZONAL	MERID.	SPEED	ZONAL	MERID.	SPEED
BRAVO	56.36	-0.314	0.212	3.365	0.786	0.750	0.601	0.138	-0.673	0.159
JULIET	53.48	-0.902	-1.191	1.212	0.848	0.814	0.923	0.338	-0.137	-0.636
PAPA	50.58	-0.502	-1.013	1.777	0.738	0.812	0.792	0.192	-0.132	-0.400
DELTA	45.37	-1.435	-1.056	2.989	0.749	0.798	0.635	0.502	0.412	0.104
VICTOR	34.11	-0.983	-0.696	1.962	0.762	0.721	0.651	0.376	-0.311	0.208
NOVEMBER 2	31.45	-0.750	0.241	1.936	0.784	0.785	0.597	-0.256	-1.442	0.387
NOVEMBER 1	29.06	1.350	0.409	2.364	0.709	0.674	0.585	-0.683	-1.370	-0.242

TABLE VIII

Coefficients for regression of observed time series on computed time series for each Ocean Station.

SERIES	GRID PT. LAT. N	B_0			B_1			B_2 X 100		
		ZONAL	MERID.	SPEED	ZONAL	MERID.	SPEED	ZONAL	MERID.	SPEED
BRAVO	56.36	-0.322	0.432	4.461	0.872	0.787	0.584	0.213	-0.041	0.169
JULIET	53.48	-0.412	0.852	3.121	0.879	0.901	0.694	0.304	-0.007	-0.261
PAPA	50.58	-1.071	0.401	3.380	0.943	0.866	0.823	0.195	0.175	-0.597
DELTA	45.37	-0.344	0.246	4.556	0.875	0.818	0.563	0.097	0.058	0.225
VICTOR	34.11	0.162	0.359	3.100	0.866	0.880	0.739	0.250	0.020	-0.533
NOVEMBER 2	31.45	1.701	0.310	2.913	0.758	0.772	0.666	-0.147	-0.162	-0.763
NOVEMBER 1	29.06	0.207	0.075	3.336	0.857	0.848	0.531	-0.661	0.312	0.021

TABLE IX

Scatter diagram symbols (for Figures 11 and 12) and the corresponding number of coincident computed and observed wind speed pairs.

Diagram Symbol	Equivalent Values		
1	1	J	20
2	2	K	21
3	3	L	22
4	4	M	23
5	5	N	24
6	6	O	26
7	7	P	27
8	8	Q	29
9	9	R	33
+	10	S	41
A	11	T	57
B	12	U	89
C	13	V	153
D	14	W	281
E	15	X	537
F	16	Y	1049
G	17	Z	2073
H	18	*	$\geq$4121
I	19		

TABLE X

Ratio of surface wind speed (V_S) to geostrophic wind speed (V_g) and deflection angle (in degrees) at low latitudes as tabulated by Brümmer, et al. and as formulated in the model.

LATITUDE	V_s/V_g		Deflection Angle	
	BRUMMER	MODEL	BRUMMER	MODEL
18	.60	.74	13	25
15	.74	.72	21	26
10	.60	.68	27	28
2	.60	.62	55	32

TABLE XI

Autocorrelation of observed and computed time series at Ocean Station Bravo and Ocean Station Victor at selected frequencies.

PERIOD (DAYS)	FREQ. (DAY $^{-1}$)	BRAVO						VICTOR					
		ZONAL		MERIDIONAL		SPEED		ZONAL		MERIDIONAL		SPEED	
		OBS.	COMP.	OBS.	COMP.	OBS.	COMP.	OBS.	COMP.	OBS.	COMP.	OBS.	COMP.
2.0	.5000	0.400	0.458	0.309	0.341	0.291	0.275	0.479	0.511	0.079	0.121	0.427	0.333
4.0	.2500	0.211	0.237	0.193	0.170	0.208	0.187	0.360	0.381	0.043	0.030	0.335	0.276
7.0	.1432	0.113	0.123	0.113	0.112	0.239	0.193	0.303	0.300	0.090	0.070	0.310	0.269
29.6	.0338	0.039	0.021	0.044	0.047	0.184	0.166	0.149	0.172	0.015	0.013	0.247	0.187
185.0	.0054	0.036	0.020	-.032	-.011	-.186	-.143	-.060	-.106	-.026	0.003	-.252	-.220
370.0	.0027	0.000	-.030	0.084	0.049	0.175	0.142	0.262	0.263	0.053	0.062	0.265	0.227

TABLE XII

Energy density (in m^2 sec^{-2}) of observed and computed time series for Ocean Station Bravo and Ocean Station Victor at selected frequencies.

PERIOD (DAYS)	FREQ. (DAY $^{-1}$)	BRAVO						VICTOR					
		ZONAL		MERIDIONAL		SPEED		ZONAL		MERIDIONAL		SPEED	
		OBS.	COMP.	OBS.	COMP.	OBS.	COMP.	OBS.	COMP.	OBS.	COMP.	OBS.	COMP.
2.0	.5000	0.002	0.002	0.002	0.002	0.001	0.001	0.002	0.001	0.002	0.001	0.002	0.001
4.0	.2500	0.070	0.048	0.057	0.051	0.028	0.031	0.036	0.033	0.058	0.034	0.016	0.022
7.0	.1432	0.152	0.122	0.112	0.101	0.067	0.068	0.063	0.052	0.051	0.059	0.030	0.024
29.6	.0338	0.478	0.485	0.347	0.471	0.113	0.106	0.190	0.193	0.168	0.152	0.053	0.053
185.0	.0054	0.683	0.612	0.691	0.619	0.353	0.318	1.393	1.177	0.149	0.181	0.338	0.245
370.0	.0027	1.123	0.990	0.997	1.113	1.303	1.186	2.038	2.057	0.279	0.187	1.124	1.066

TABLE XIII

Coherence between observed and computed time series for Ocean Station Bravo and Ocean Station Victor at selected frequencies.

PERIOD (DAYS)	FREQ. (DAY $^{-1}$)	BRAVO			VICTOR		
		ZONAL	MERID.	SPEED	ZONAL	MERID.	SPEED
2.0	.5000	.705	.501	.562	.430	.686	.624
4.0	.2500	.790	.750	.692	.780	.856	.780
7.0	.1432	.855	.806	.760	.742	.814	.522
29.6	.0338	.927	.812	.705	.943	.888	.783
185.0	.0054	.943	.927	.889	.970	.804	.731
370.0	.0027	.920	.946	.963	.978	.770	.937

TABLE XIV

Phase difference (in degrees) between observed and computed time series for Ocean Station Bravo and Ocean Station Victor at selected frequencies.

PERIOD (DAYS)	FREQ. (DAY $^{-1}$)	BRAVO			VICTOR		
		ZONAL	MERID.	SPEED	ZONAL	MERID.	SPEED
2.0	.5000	0.3	29.2	39.9	-9.8	-8.2	2.6
4.0	.2500	8.0	29.0	14.9	-7.2	4.5	5.6
7.0	.1432	14.2	7.1	-12.3	-19.7	-4.9	-4.4
29.6	.0338	1.7	0.1	11.2	0.9	12.0	-1.5
185.0	.0054	-0.6	-3.2	-2.6	-3.7	-3.4	-0.2
370.0	.0027	-5.6	-5.9	-3.5	-1.7	-15.1	8.2

Figure 1. Latitude dependence of the ratio of the surface wind speed (V_S) to the geostrophic wind speed (V_g) as found by Roll (broken line), Carstensen (solid line) and as formulated in the model (dashed line).

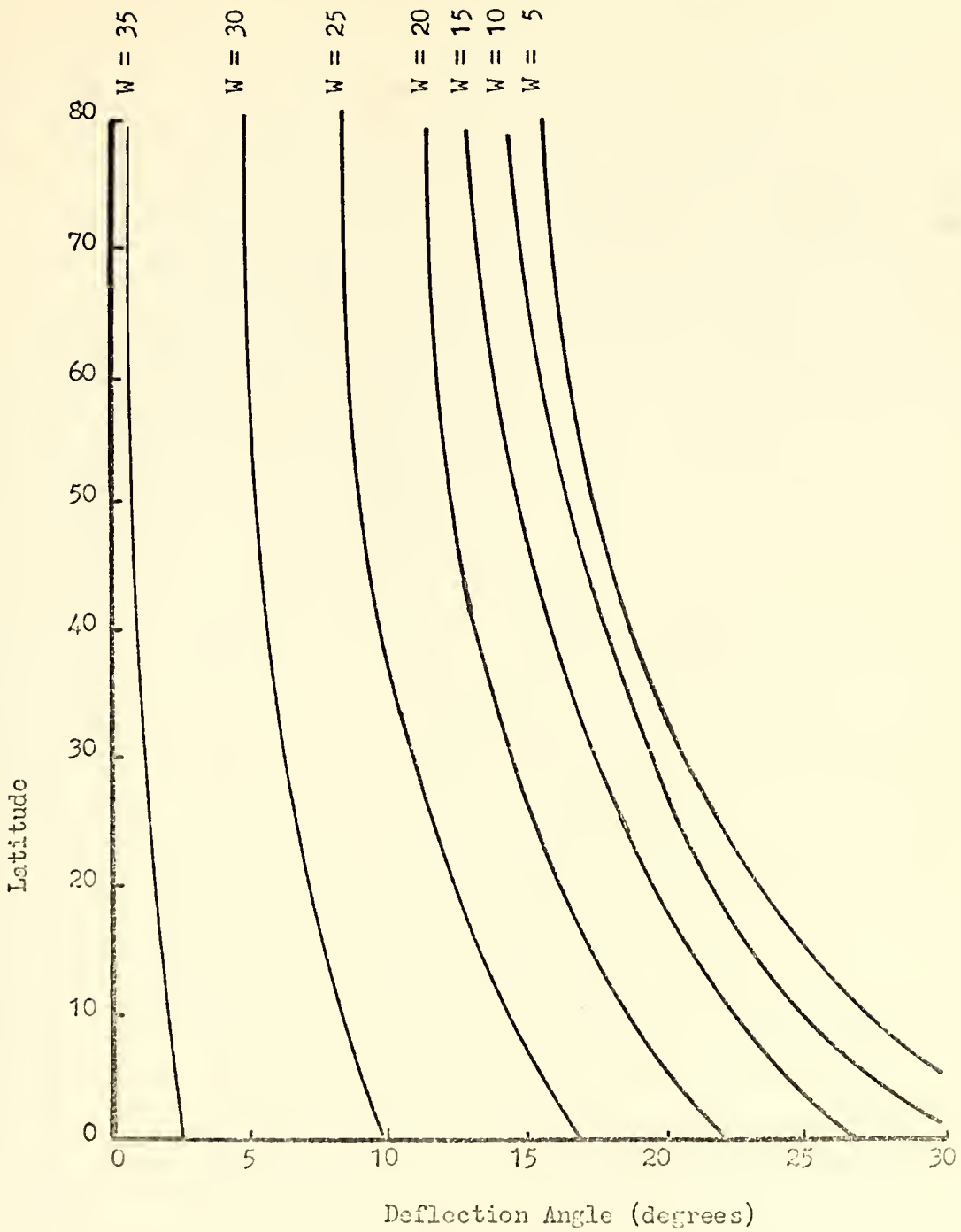

Figure 2. Latitude dependence of the deflection angle for various wind speeds (W in m sec^{-1}) as formulated in the model.

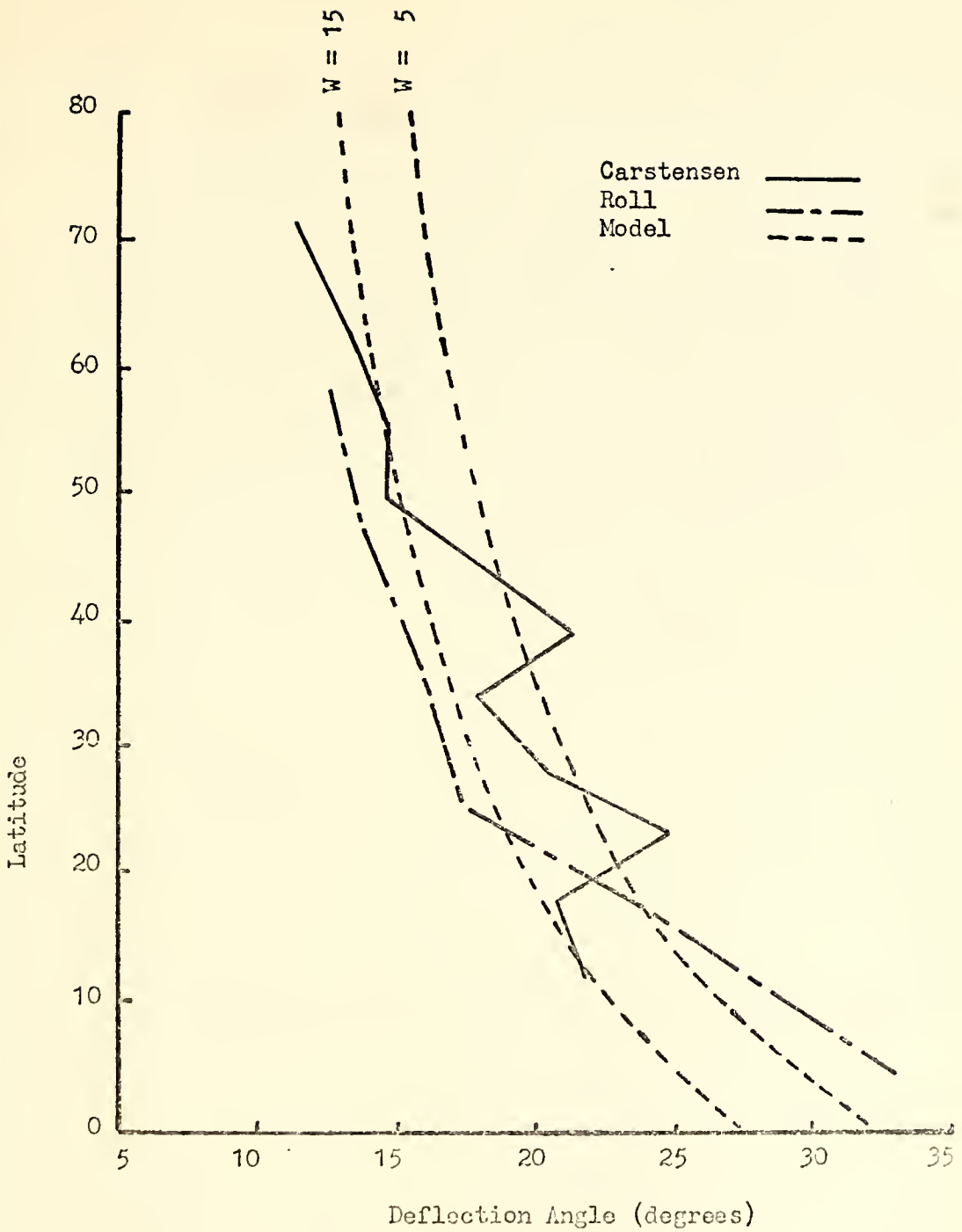

Figure 3. Latitude dependence of the deflection angle as found by Roll (broken line), Carstensen (solid line), and as formulated in the model for wind speeds (W) of 5 m sec^{-1} and 15 m sec^{-1} (dashed lines).

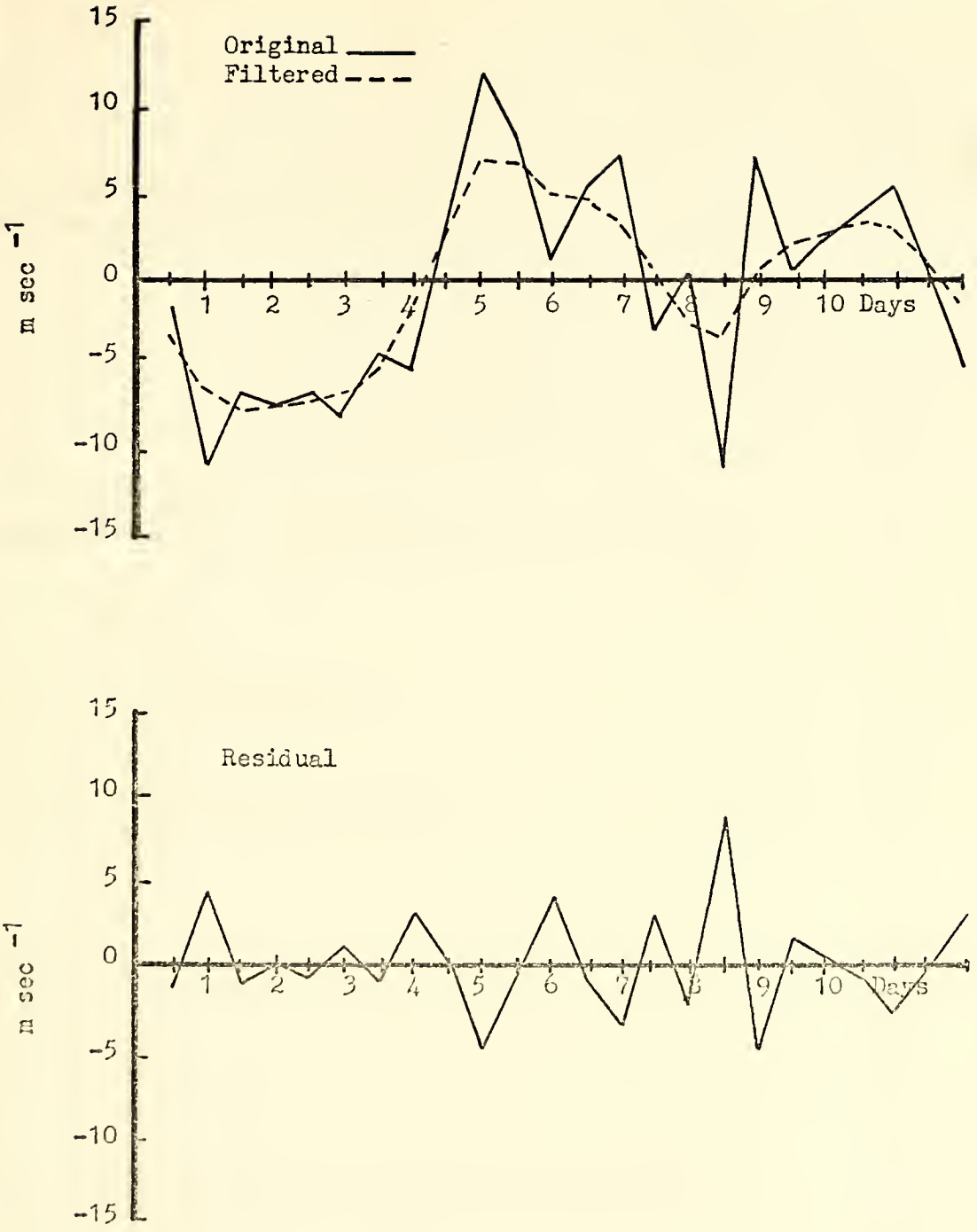

Figure 4. Result of five point binomial filter applied to a typical portion of a zonal component time series. Original series (solid line) and filtered series (dashed line) are shown in the upper graph. The residual series is shown in the lower graph.

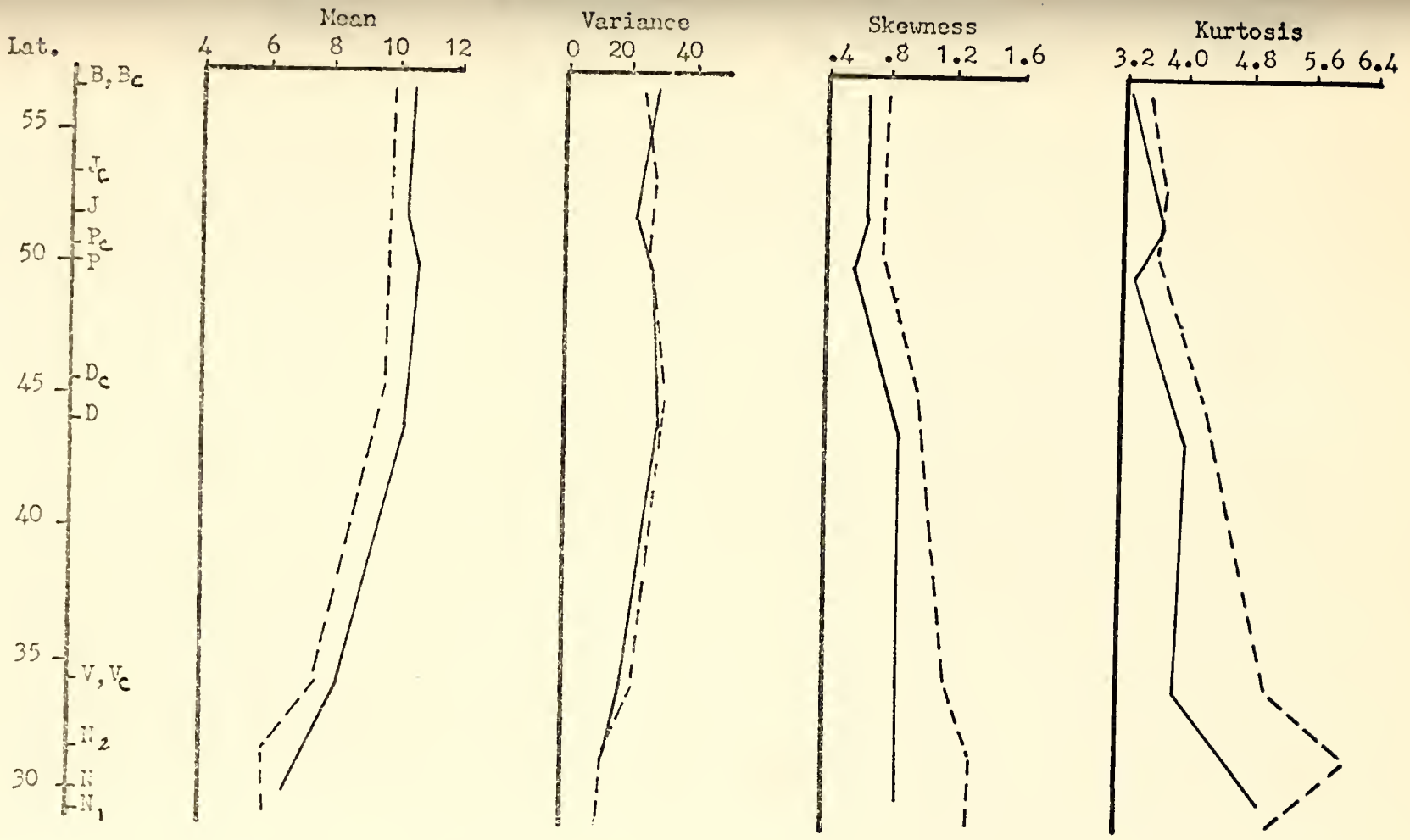

Figure 5. Central moments of the distributions of observed (solid line) and computed (dashed line) wind speeds. (Mean wind speed in m sec-1; variance in m^2 sec^{-2}).

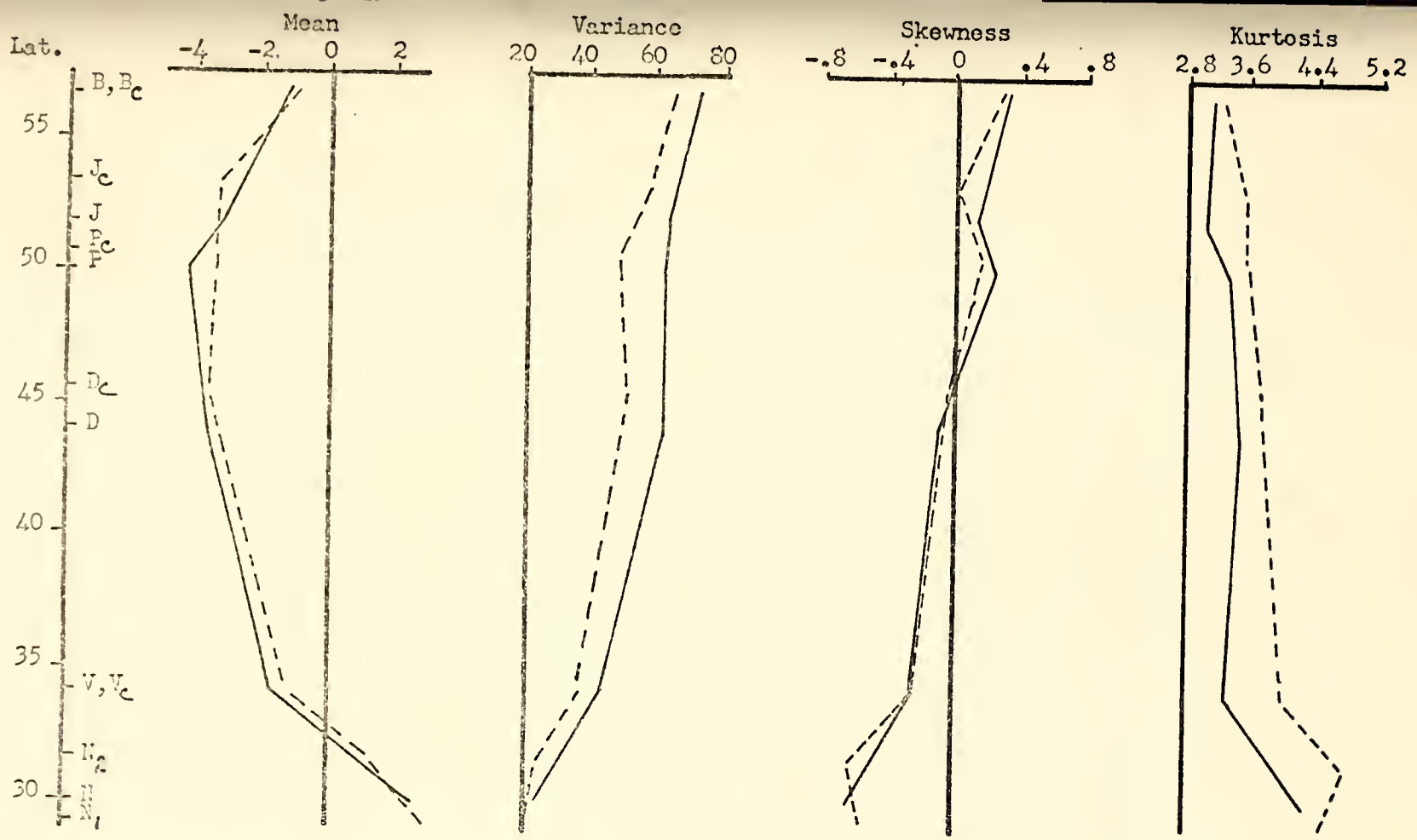

Figure 6. Central moments of the distribution of observed (solid line) and computed (dashed line) zonal components. (Mean zonal component in m sec-1; variance in m^2 sec^{-2}).

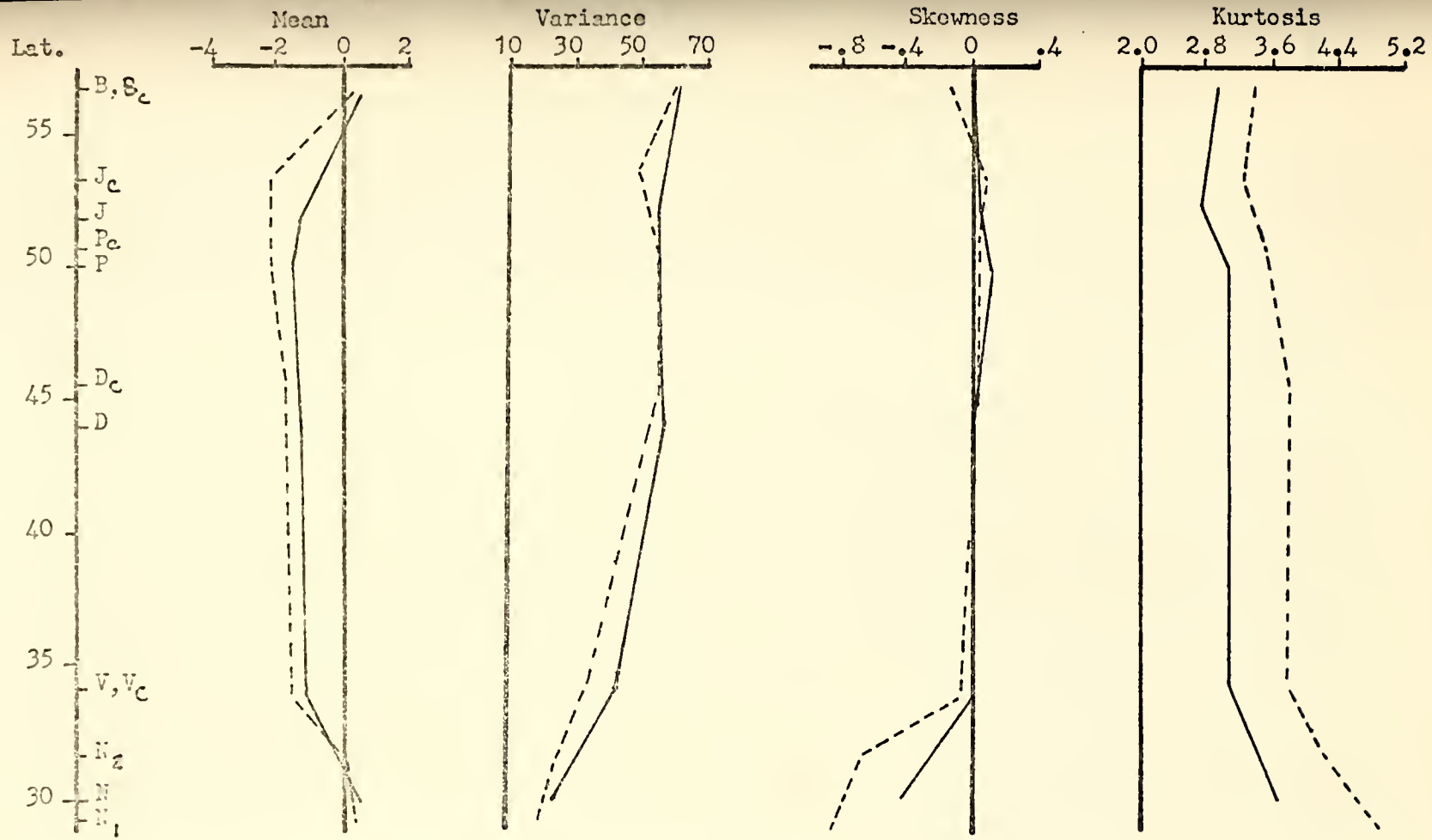

Figure 7. Central moments of the distributions observed (solid line) and computed (dashed line) meridional components. (Mean meridional component in m sec^{-1}; variance in m^2 sec^{-2}.)

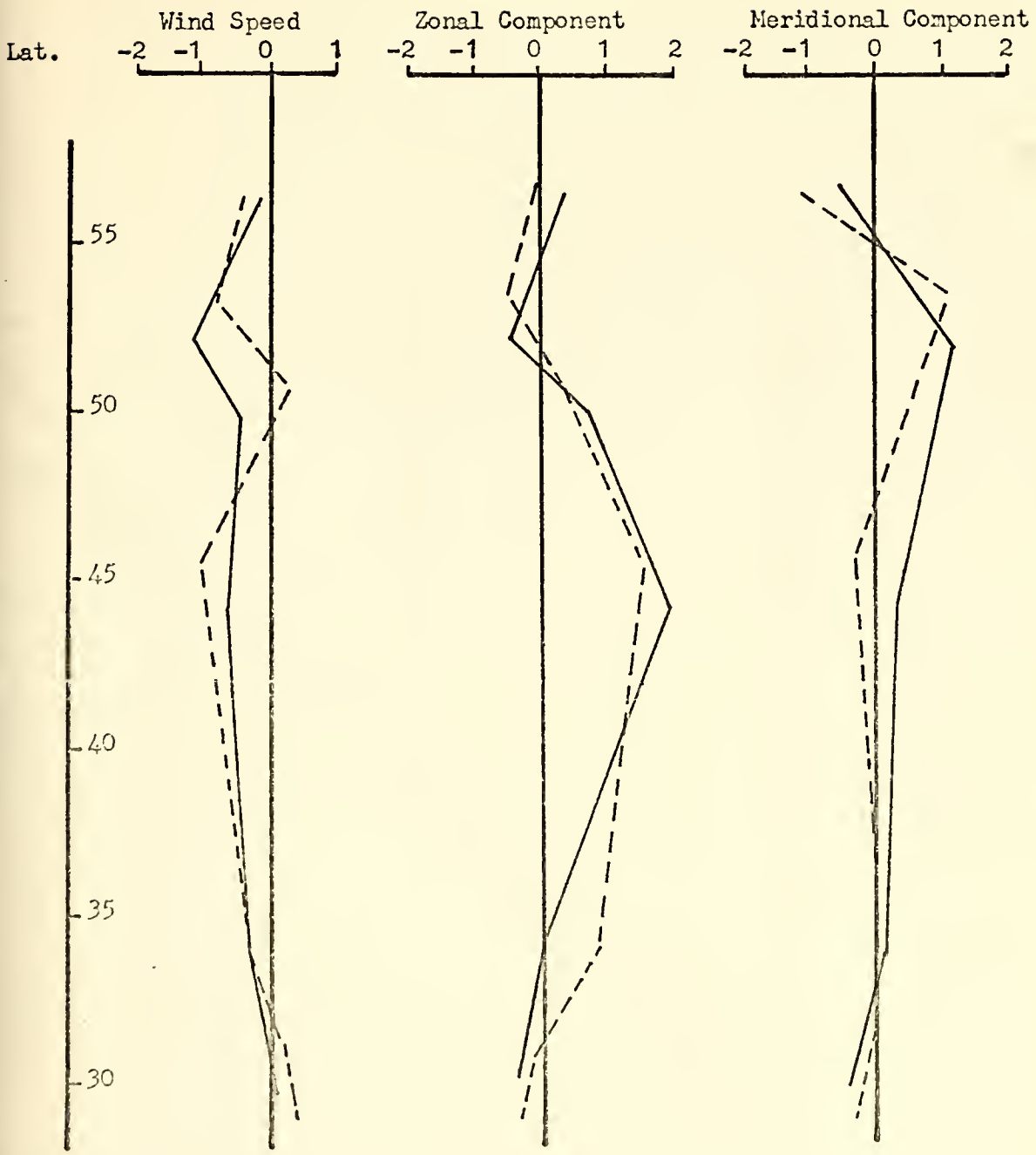

Figure 8. Total change (integrated linear trend) over the ten year period from January 1960 through December 1969 in the observed (solid line) and computed (dashed line) wind speed and zonal and meridional components (in m sec^{-1}).

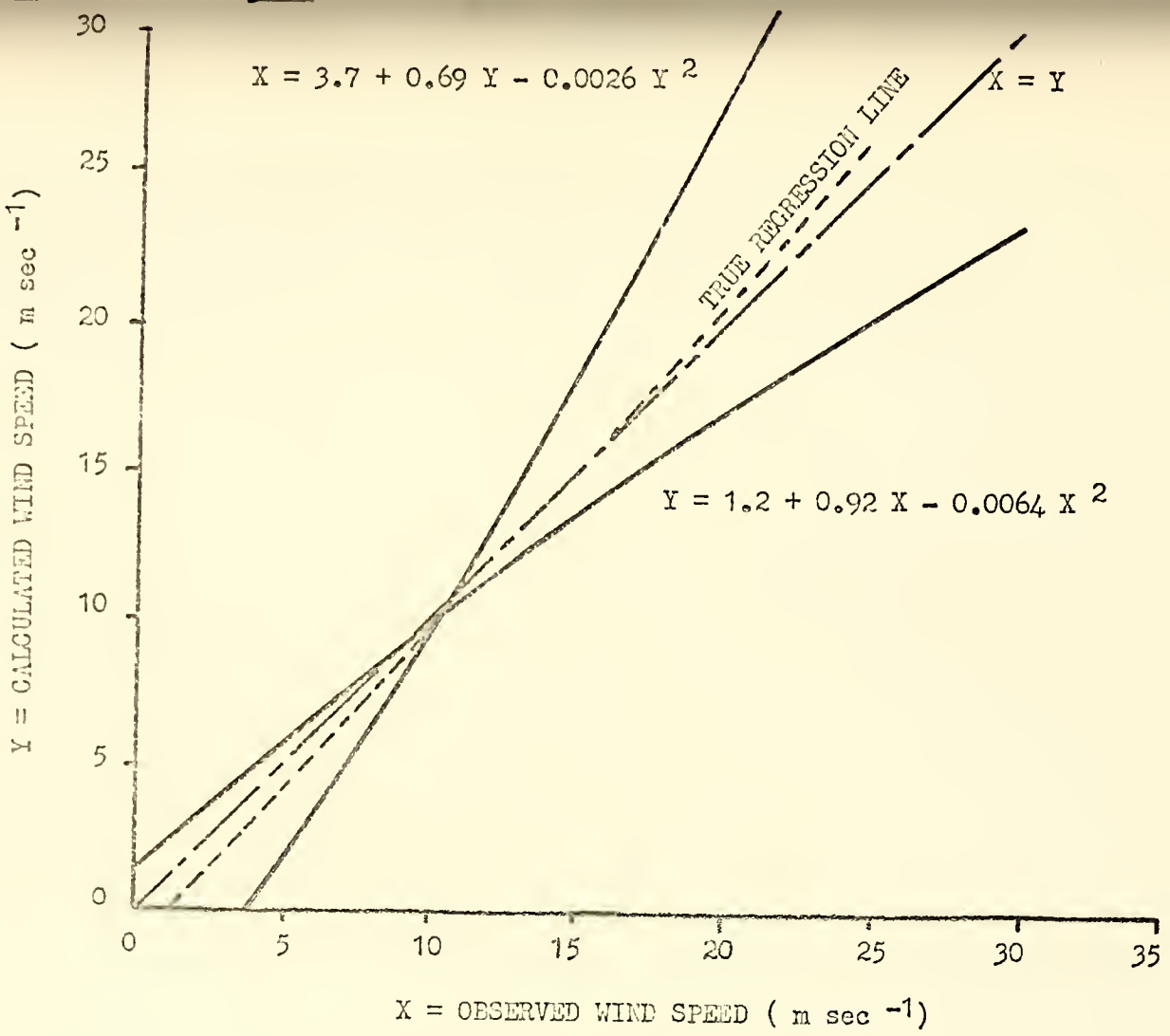

Figure 9. Regression relations between the observed and computed wind speeds for Ocean Station Juliet.

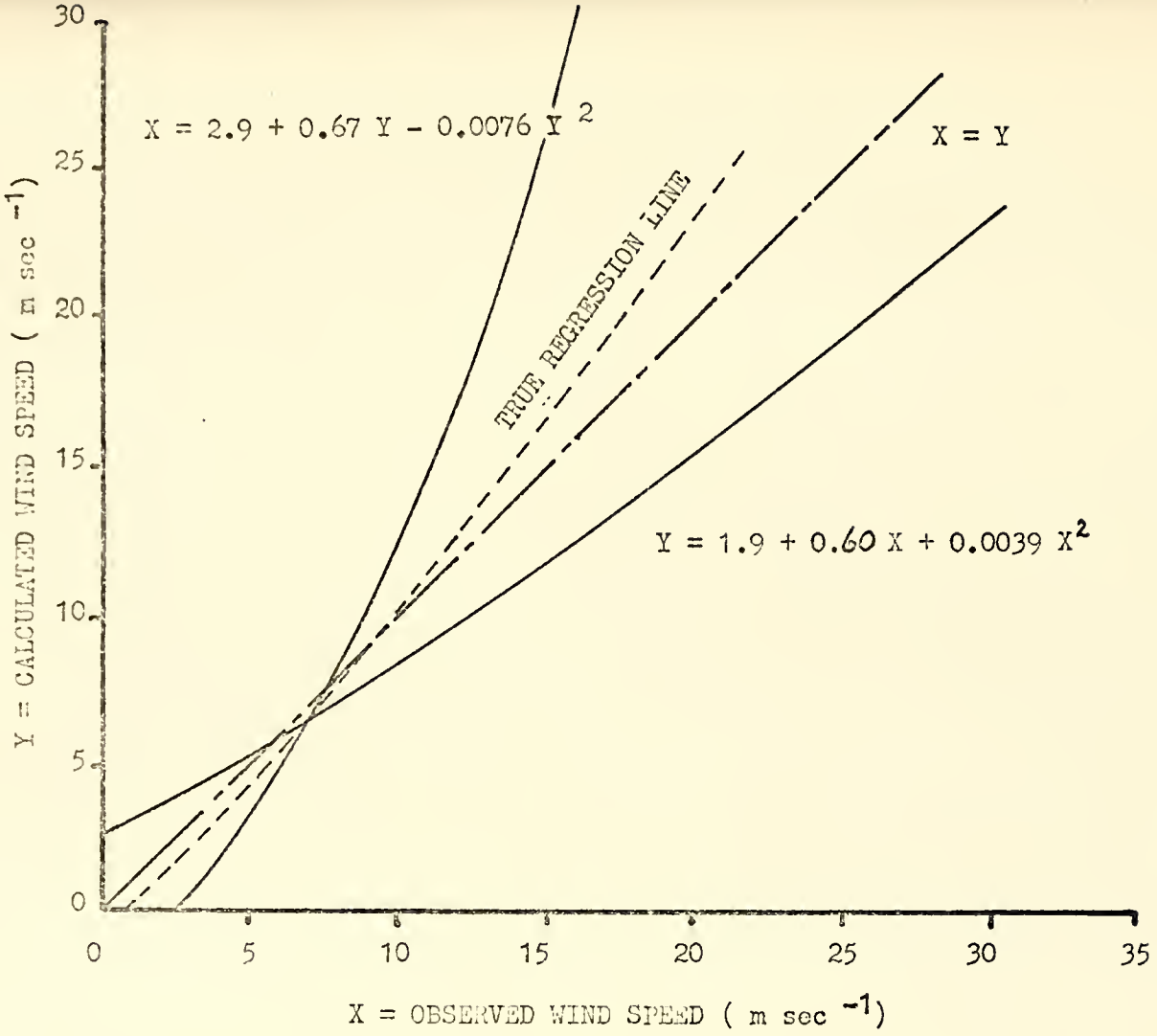

Figure 10. Regression relations between computed wind speeds for Ocean Station November.

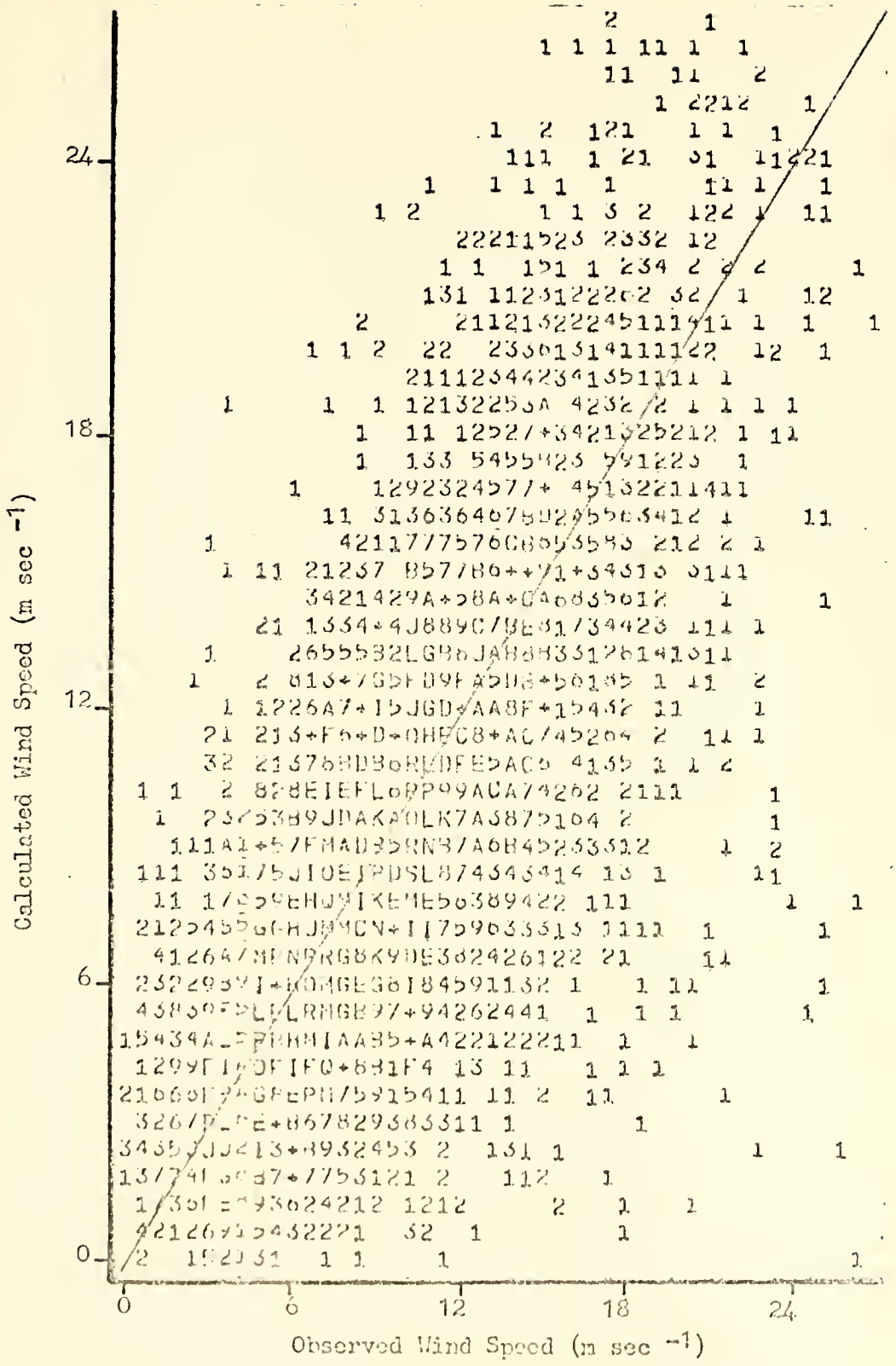

Figure 11. Scatter of observed and computed wind speeds (in m sec^{-1}) at Ocean Station Juliet. Table IX defines the symbols.

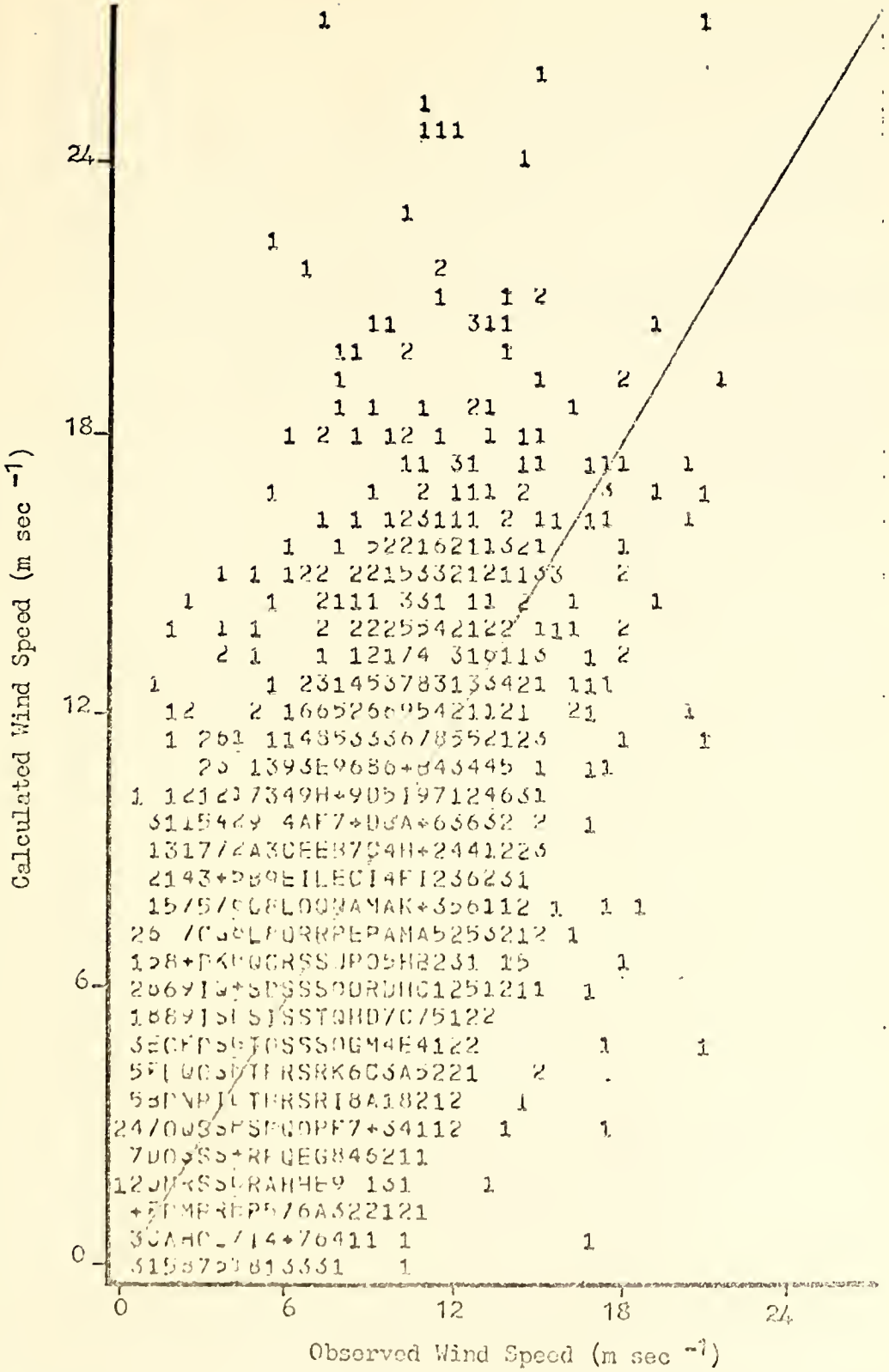

Figure 12. Scatter of observed and computed wind speeds (in m sec^{-1}) at Ocean Station November. Table IX defines the symbols.

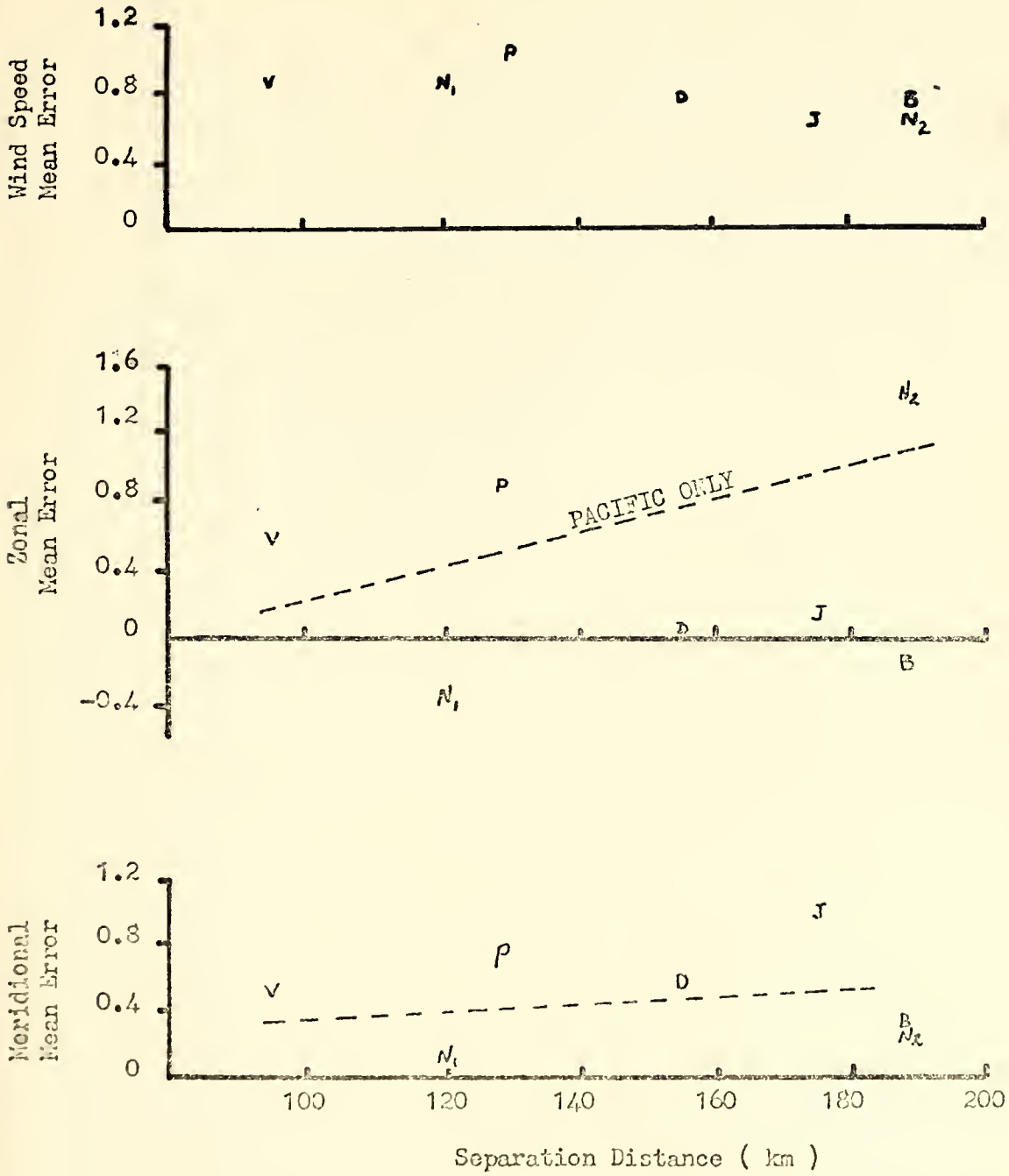

Figure 13. Mean error (in m sec^{-1}) dependence on separation distance for wind speed and the zonal and meridional components. Estimated best-fit lines are shown for components.

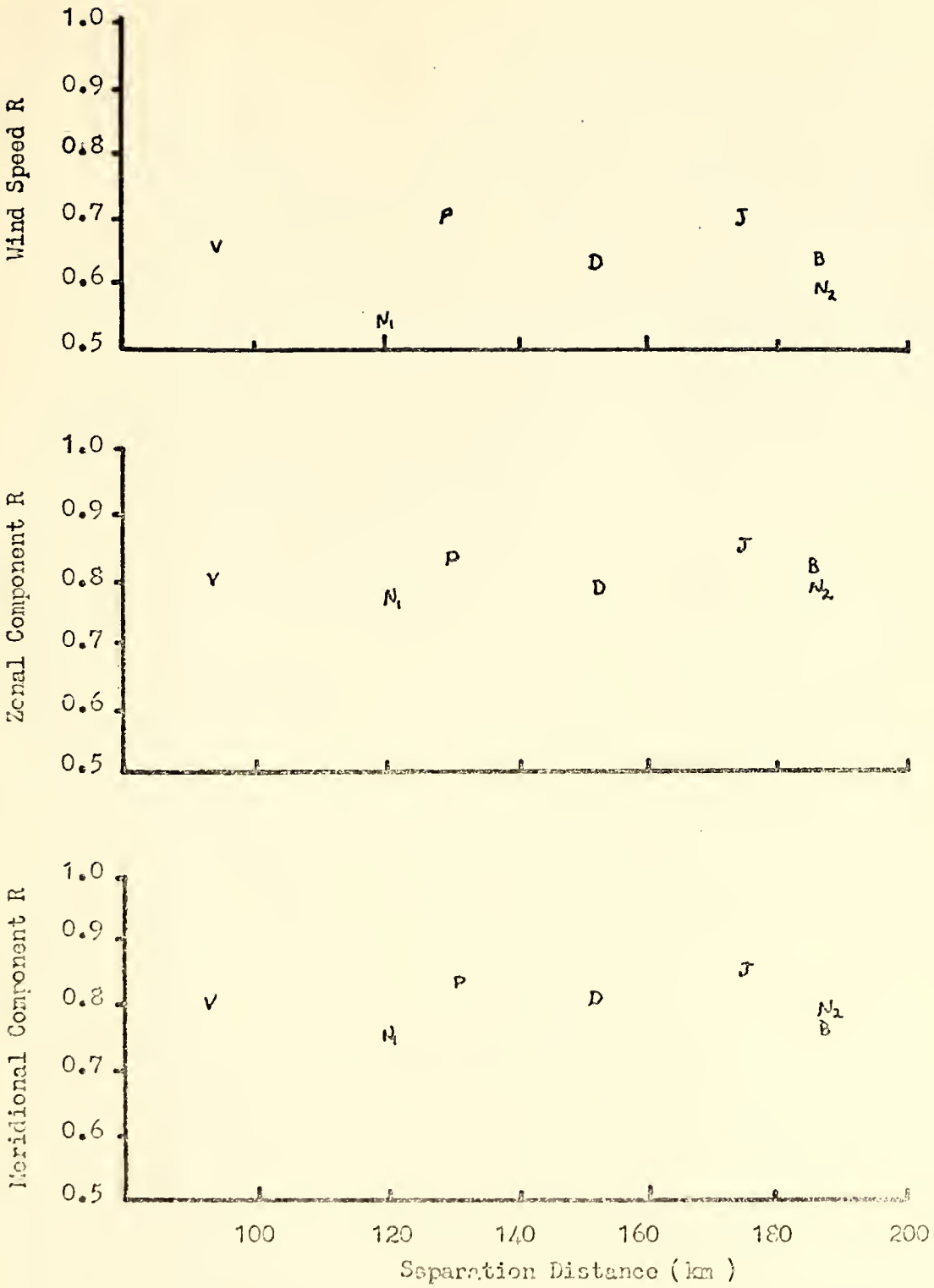

Figure 14. Linear correlation coefficient (R) dependence on separation distance for wind speed and the zonal and meridional components.

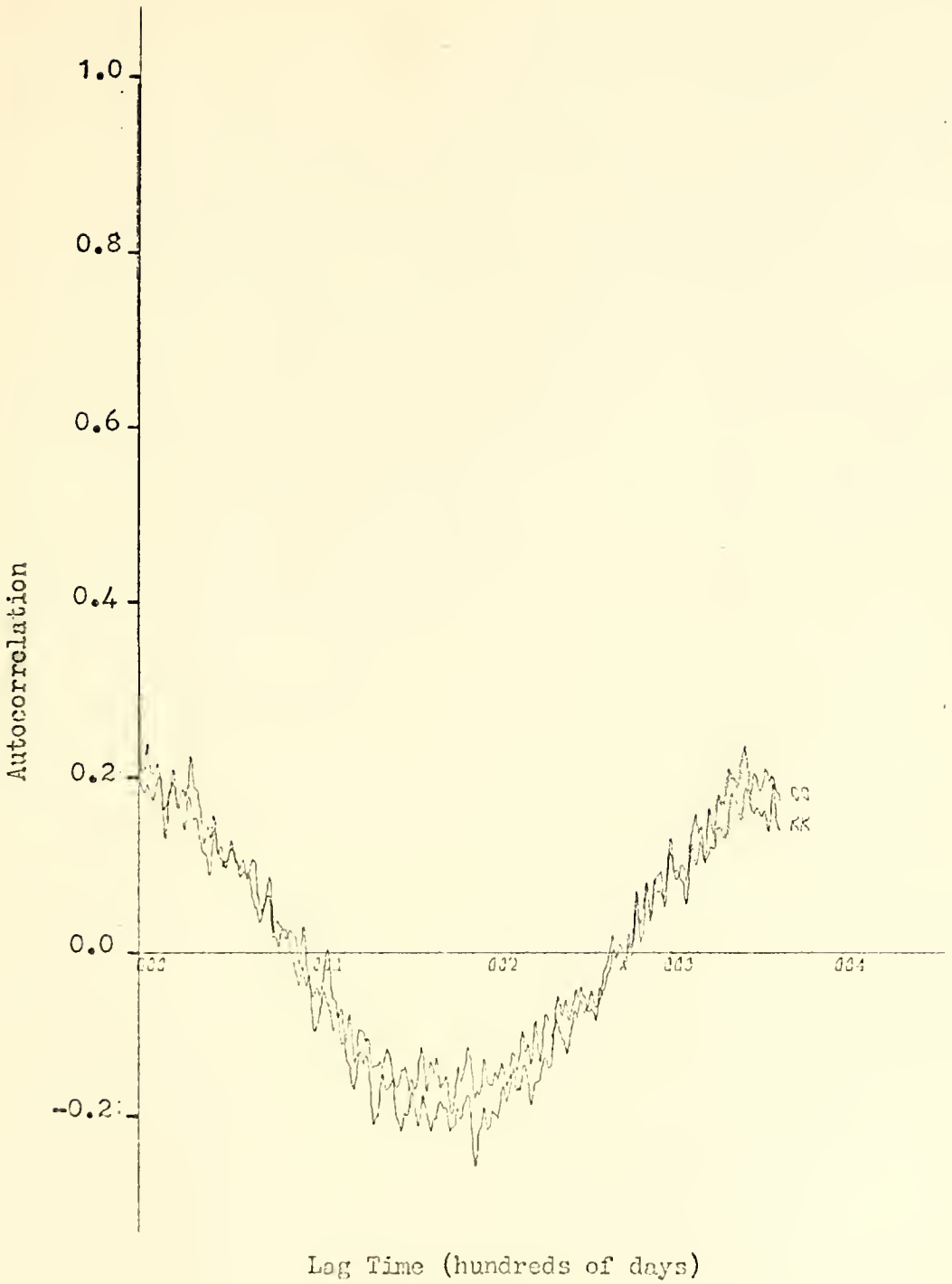

Figure 15. Autocorrelation of observed (CO) and computed (XX) wind speeds at Ocean Station Bravo.

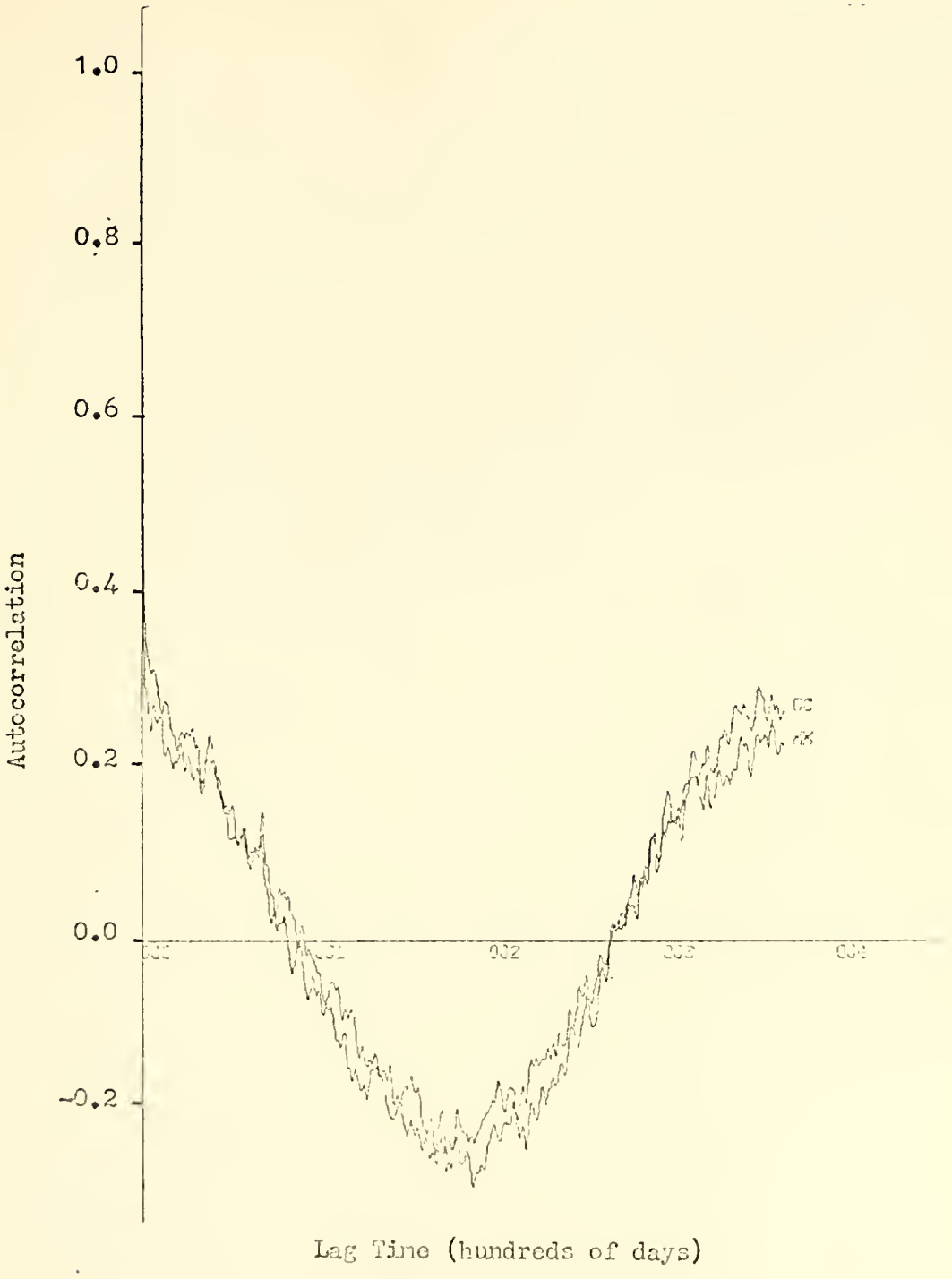

Figure 16. Autocorrelation of observed (CO) and computed (XX) wind speeds at Ocean Station Victor.

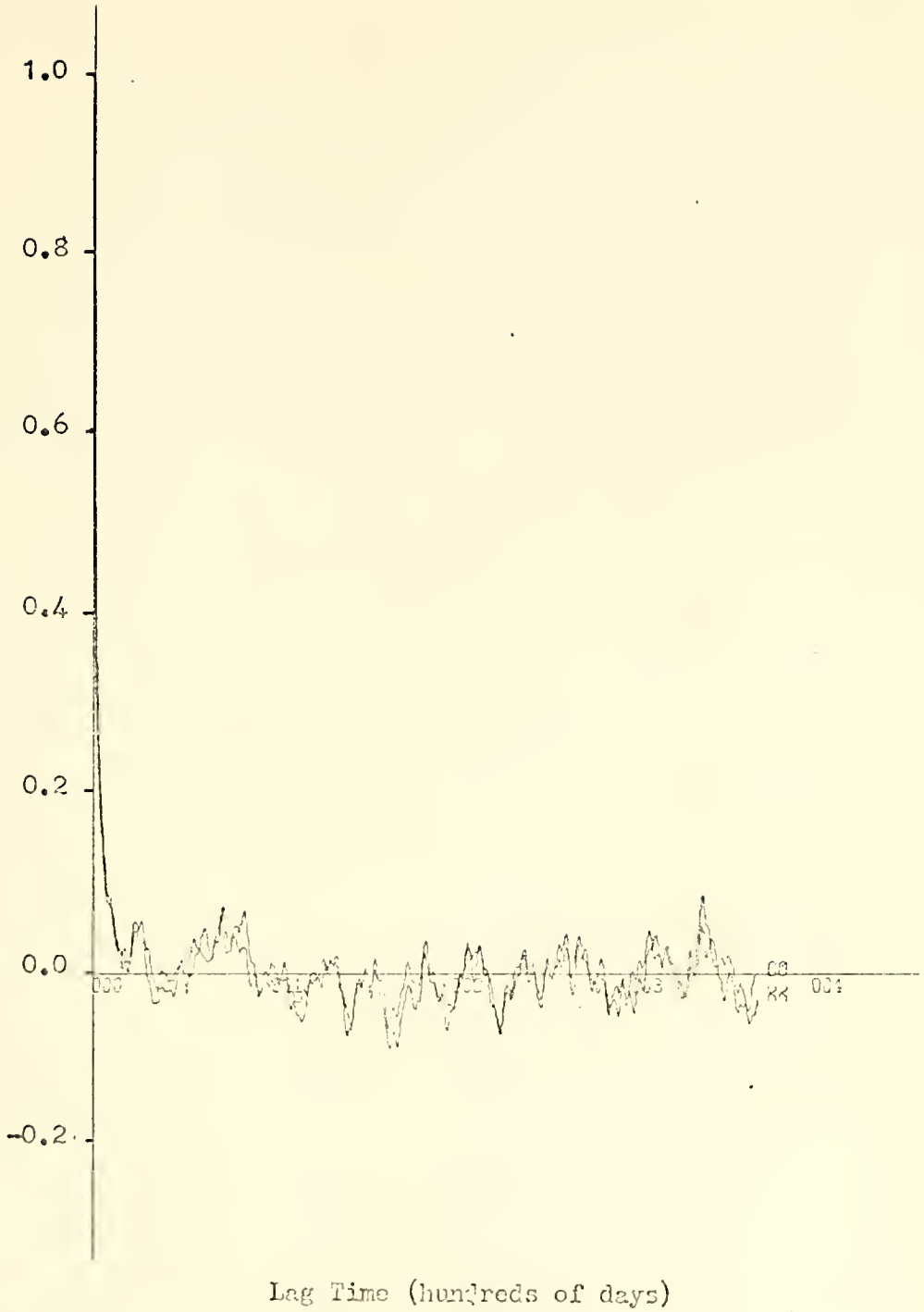

Figure 17. Autocorrelation of observed (CO) and computed (XX) zonal components at Ocean Station Bravo.

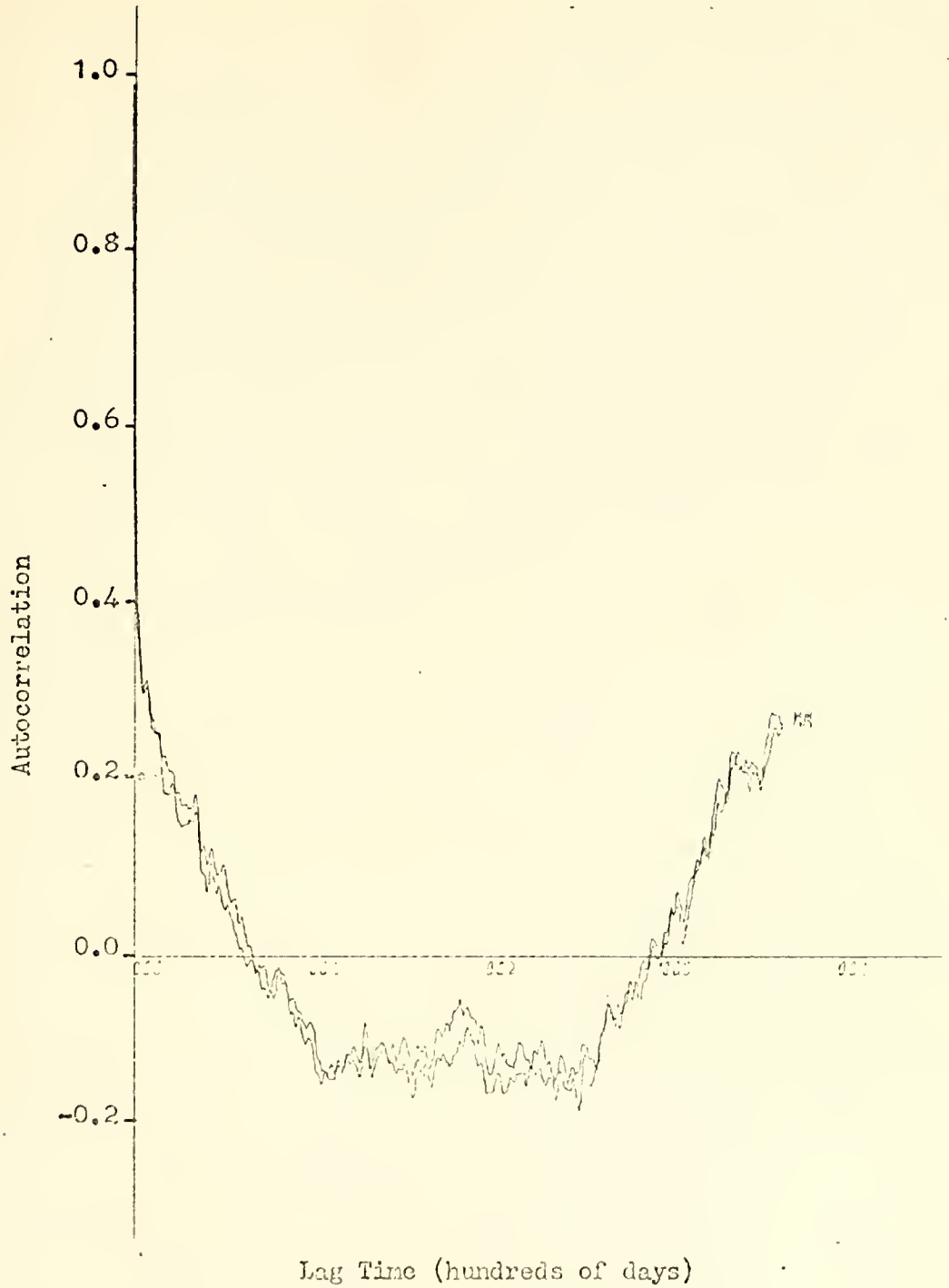

Figure 18. Autocorrelation of observed (CO) and computed (XX) zonal components at Ocean Station Victor.

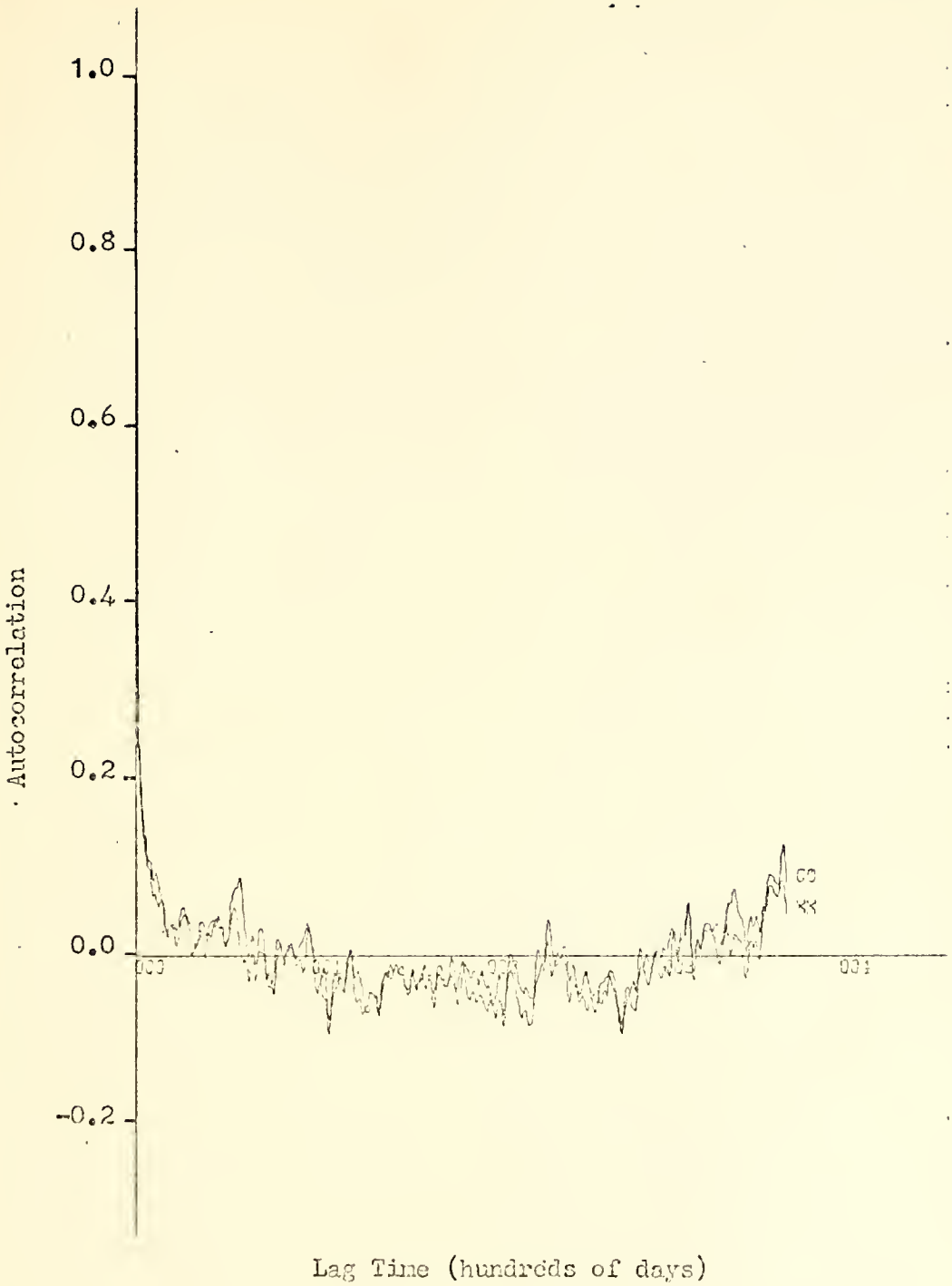

Figure 19. Autocorrelation of observed (CO) and computed (XX) meridional components at Ocean Station Bravo.

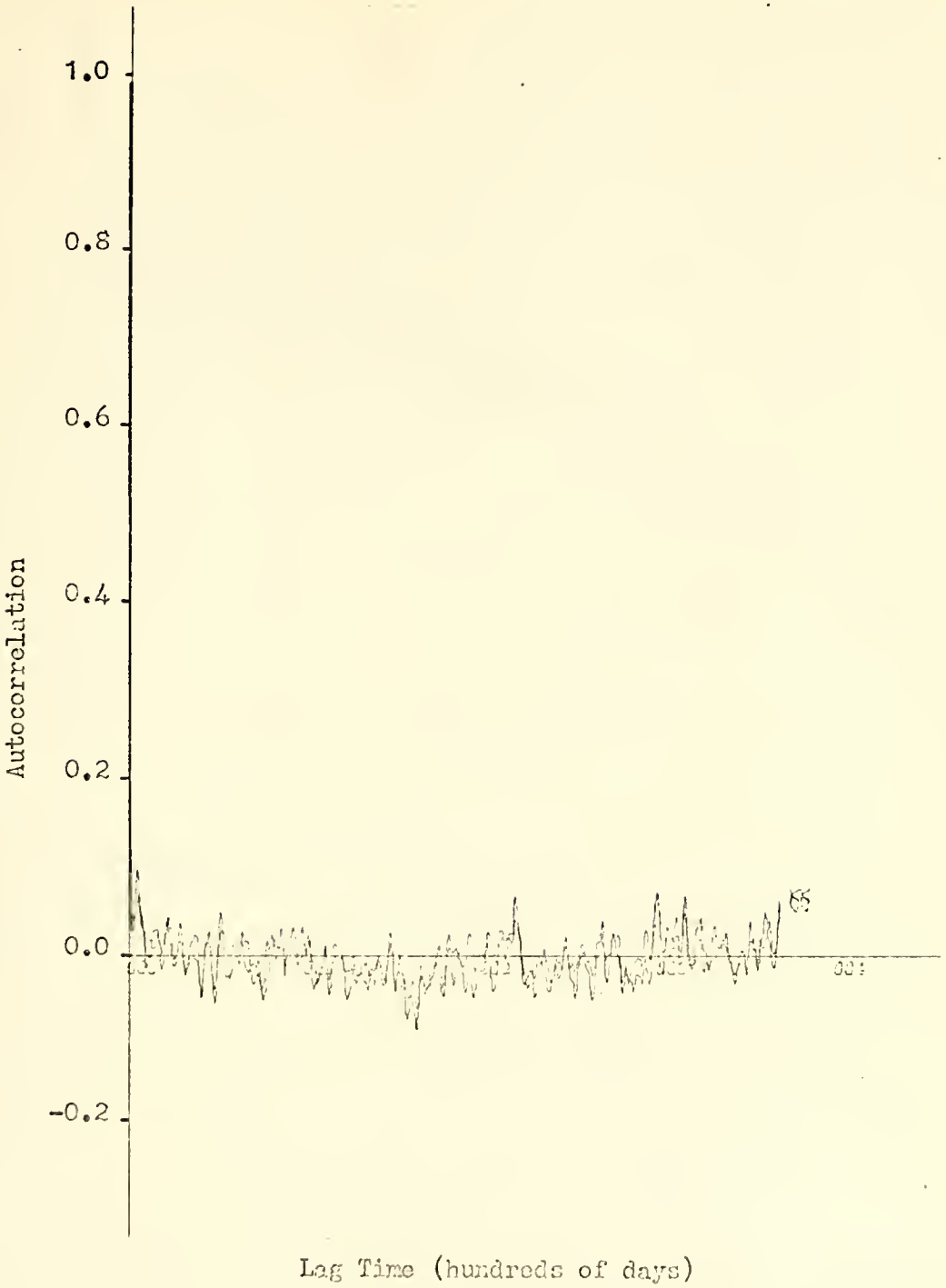

Figure 20. Autocorrelation of observed (CO) and computed (XX) meridional components at Ocean Station Victor.

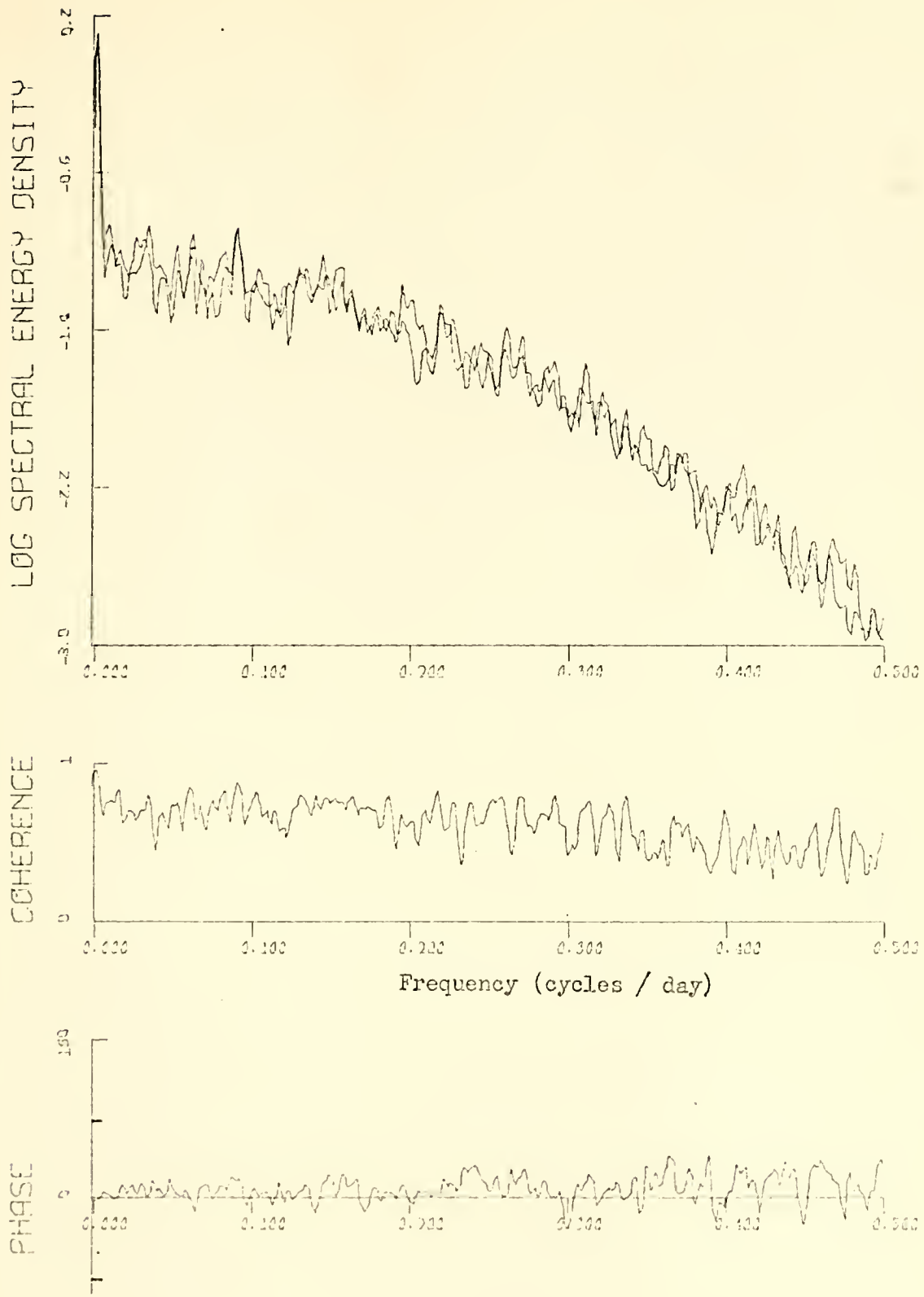

Figure 21. Log energy density (in m^2 sec^{-2}), coherence, and phase difference (in degrees) for computed and observed wind speeds at Ocean Station Bravo.

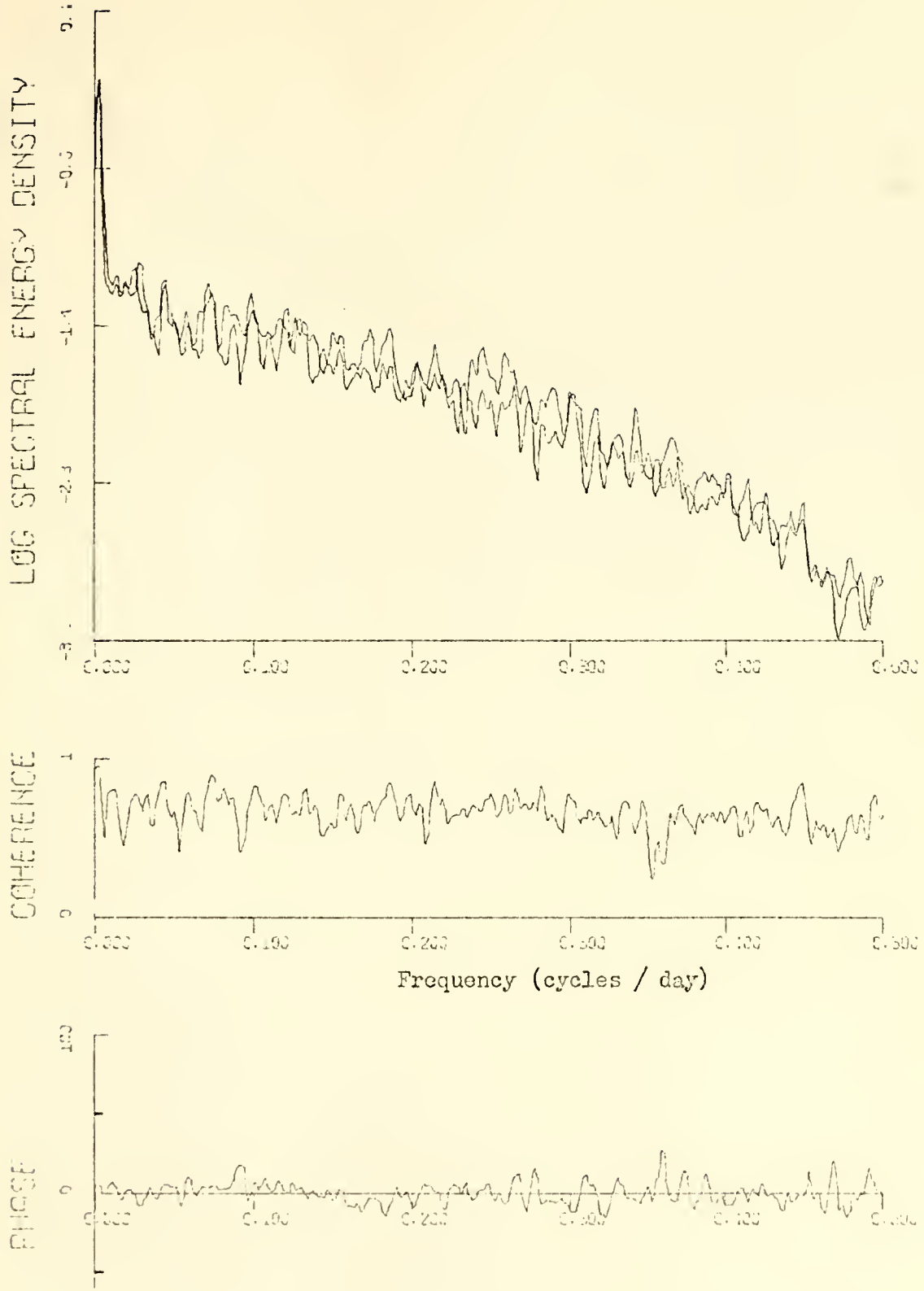

Figure 22. Log energydensity in (m^2 sec^{-2}), coherence, and phase difference (in degrees) for computed and observed wind speeds at Ocean Station Victor.

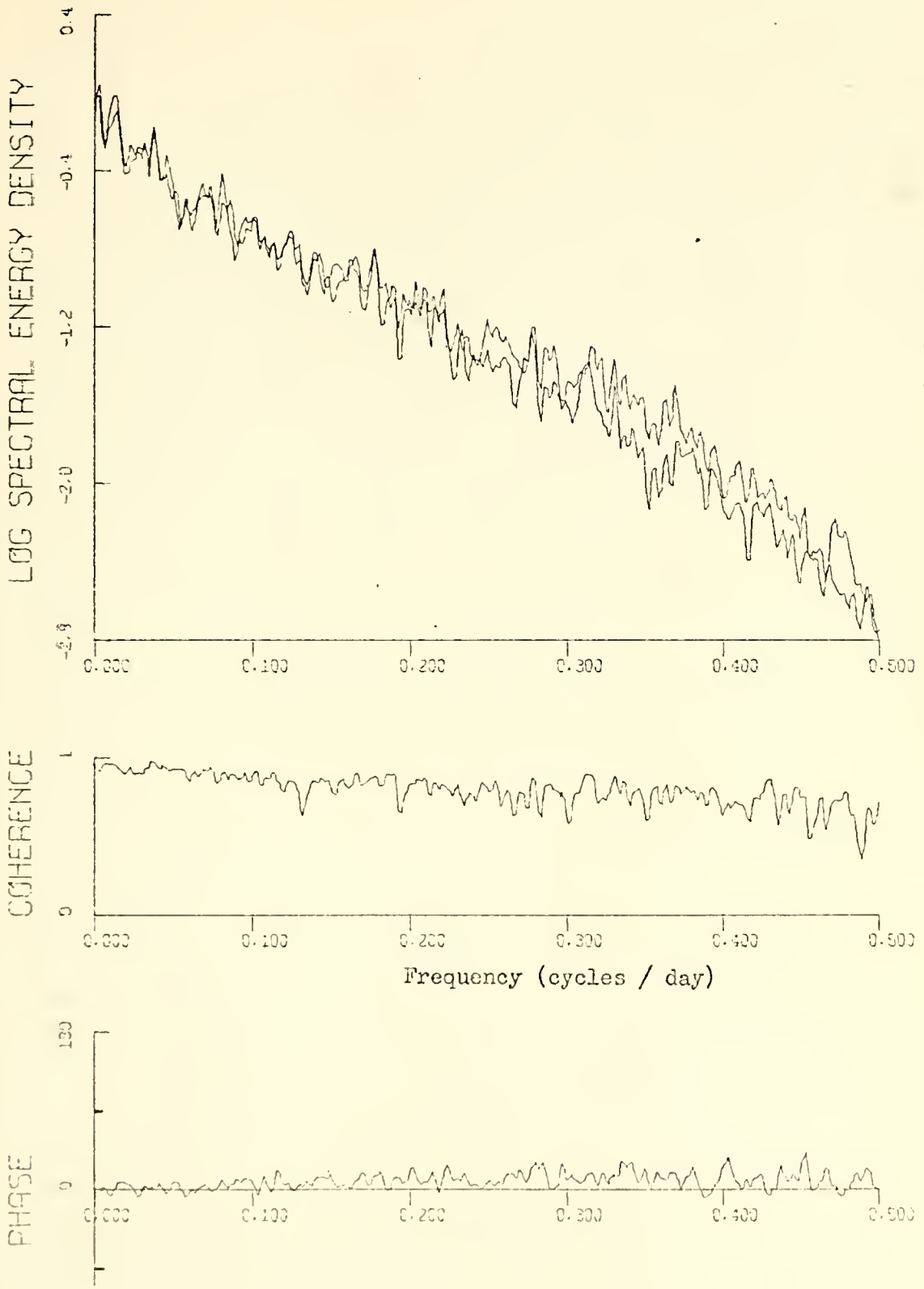

Figure 23. Log energy density (in m^2 sec^{-2}), coherence, and phase difference (in degrees) for computed and observed zonal components at Ocean Station Bravo.

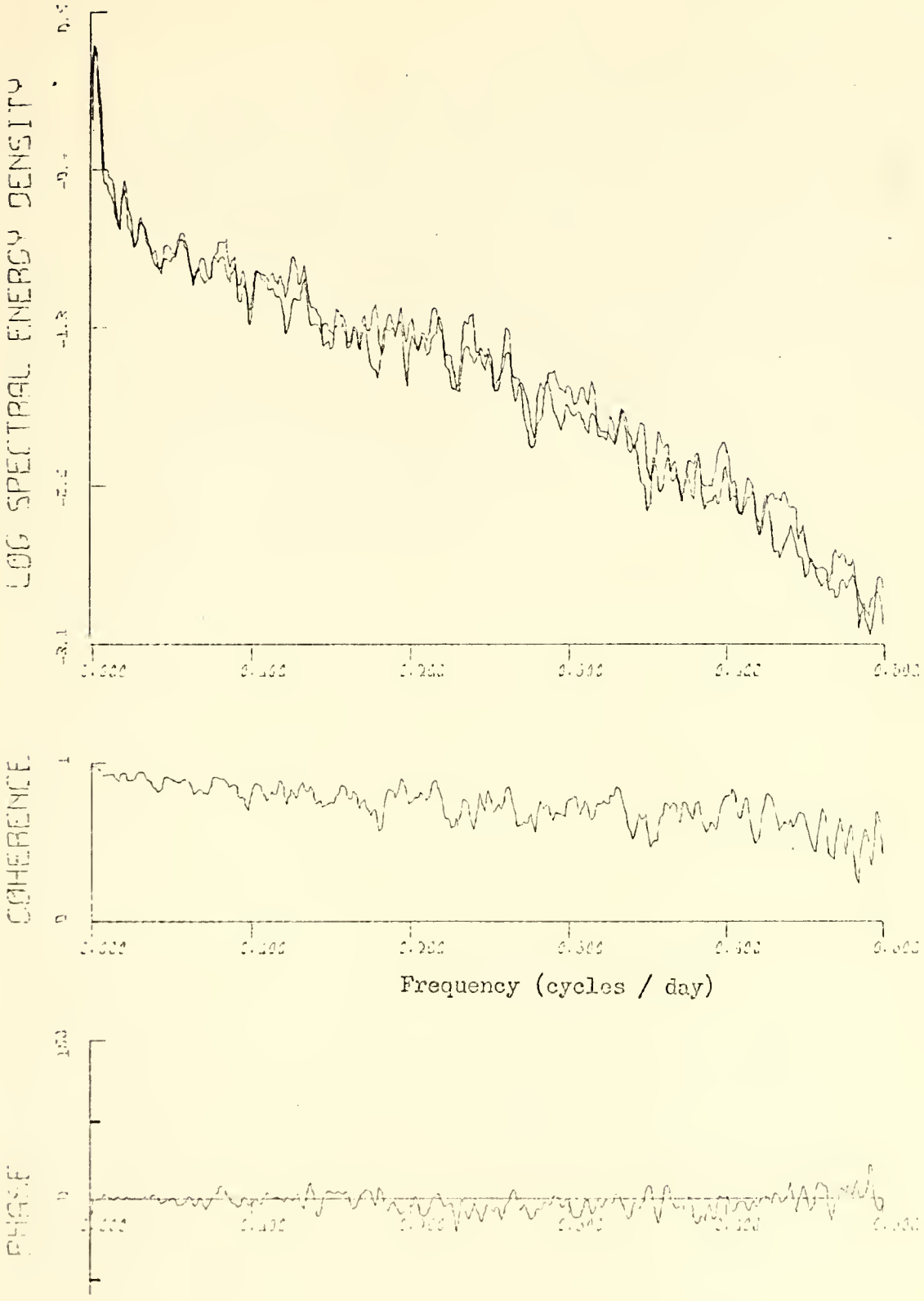

Figure 24. Log energy density (in m^2 sec^{-2}), coherence, and phase difference for computed and observed zonal components at Ocean Station Victor.

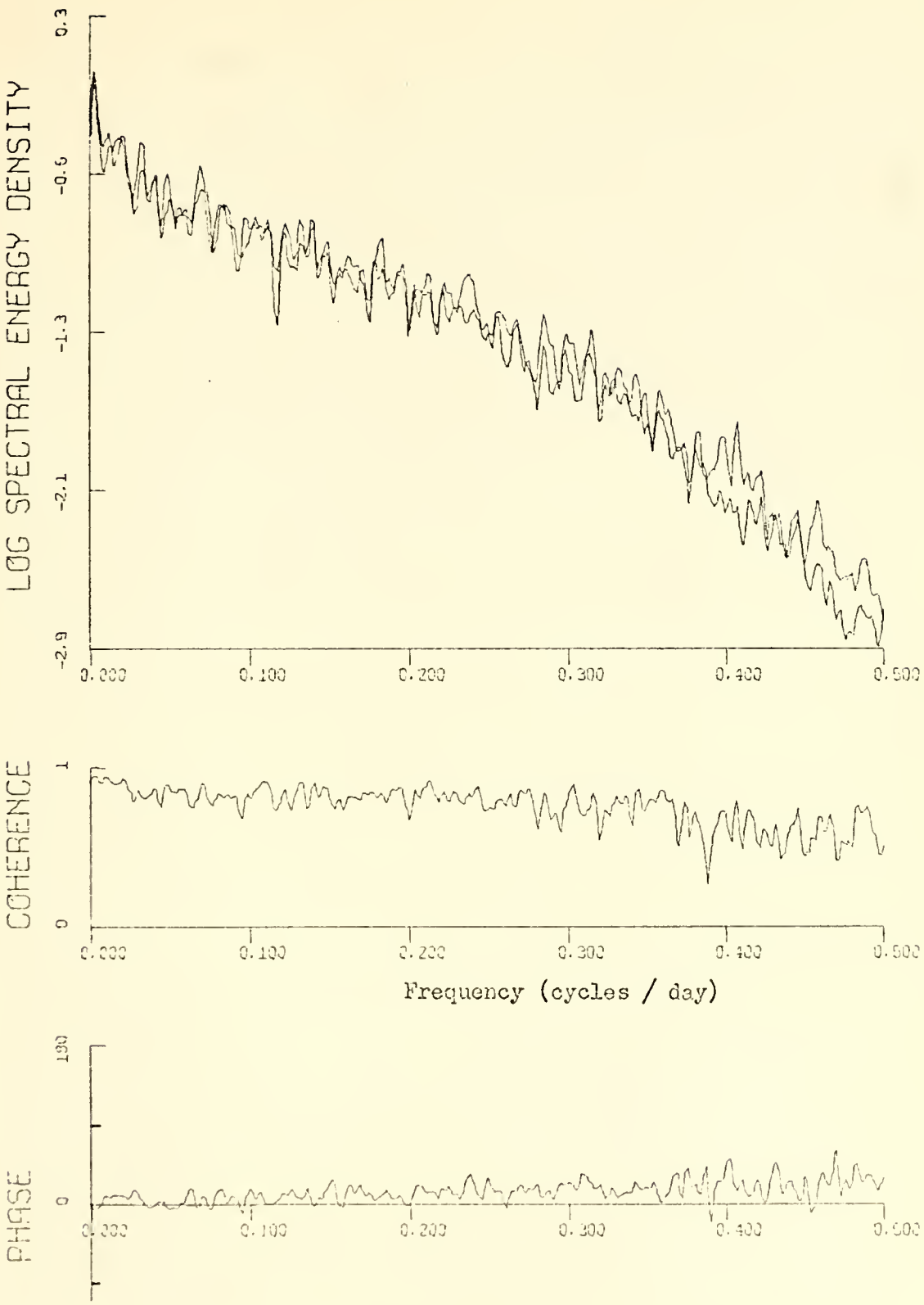

Figure 25. Log energy density (in m^2 sec^{-2}), coherence, and phase difference for computed and observed meridional components at Ocean Station Bravo.

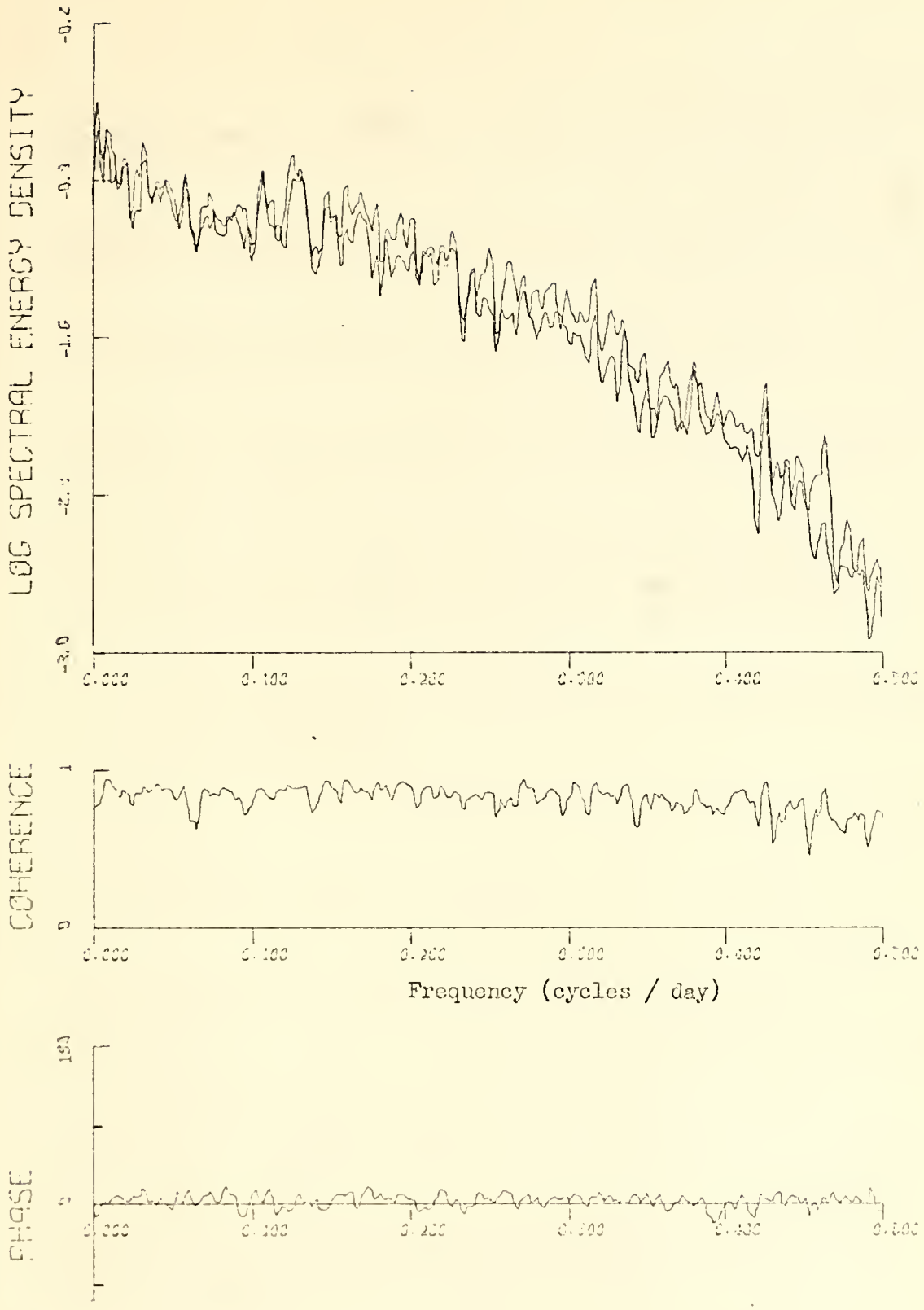

Figure 26. Log energy density in m^2 sec^{-2}), coherence and phase differences for computed and observed meridional components at Ocean Station Victor.

LIST OF REFERENCES

1. Bakun, A., 1973: Coastal Upwelling Indices, West Coast of North America 1946-71. NOAA Technical Report, NMFS SSRF-671.

2. Bendat, J. S. and A. G. Piersol, 1971: Random Data: Analysis and Measurement Procedures. Wiley-Interscience, 407 pp.

3. Bjerknes, J., 1969: Atmospheric Teleconnections from the Equatorial Pacific. Mon. Wea. Rev., 97, No. 3, p. 163-172.

4. Brümmer, B., E. Augstein, and H. Riehl, 1974: On the Low Level Wind Structure in the Atlantic Trade. Quar. Jour. Roy. Met. Soc., 100, No. 423, p. 109-121.

5. Carstensen, L. P., 1967: Some Effects of Sea-Air Temperature Difference, Latitude and Other Factors on Surface Wind-Geostrophic Wind Ratio and Deflection Angle. Fleet Numerical Weather Central Technical Note 29, Fleet Numerical Weather Central, Monterey, California.

6. Fleet Numerical Weather Central, 1974: The FNWC Computer User Guide, Edition 2. Fleet Numerical Weather Central, Monterey, California.

7. Freund, J. E., 1962: Mathematical Statistics. Prentice-Hall, 390 pp.

8. Haltiner, G. J. and F. L. Martin, 1957: Dynamical and Physical Meteorology, McGraw Hill Co., 470 pp.

9. Hasse, L., 1974: On the Surface to Geostrophic Wind Relationship at Sea and the Stability Dependence on the Resistance Law. Beit. Phys. Atmos., p. 45-55.

10. Malkus, J. S., 1962: Large Scale Interactions. In The Sea. Vol. I, M.N. Hill Ed., Interscience, p. 88-294.

11. Munk, W. H., 1960: Smoothing and Persistence. Jour. Met., 17, p. 92-93.

12. Namias, J., 1963: Large Scale Interaction Over the North Pacific from Summer 1962 Through the Subsequent Winter. Jour. Geophys. Resch., Vol. 68, No. 22, pp. 6171-6186.

13. Panofsky, H. A. and G. W. Brier, 1968: Some Applications of Statistics to Meteorology. Pennsylvania State University, 224 pp.

14. Roden, G. I., 1974: Thermohaline Structure, Fronts, and Sea-Air Energy Exchange of the Trade Wind Region East of Hawaii. Jour. Phys. Ocean. 4, No. 2, p. 168-182.

15. Roll, H. U., 1965: Physics of the Marine Atmosphere. Academic Press, 426 pp.

16. Seckel, G. R., 1970: The Trade Wind Zone Oceanography Pilot Study Part IV: The Sea Level Wind Field and Wind Stress Values July 1963 to June 1965. Bureau of Commercial Fisheries Special Scientific Report, Fisheries No. 620.

17. Spiegel, M. R., 1961: Statistics, Schaum's Outline Series. McGraw-Hill 395 pp.

18. Taylor, A., 1955: Advanced Calculus. Blaisdell, 768 pp.

19. Tennekes, H. and J. L. Lummely, 1972: A First Course in Turbulence. The MIT Press, 300 pp.

20. Verploegh, G., 1967: Observation and Analysis of the Surface Wind Over the Ocean. Koninklijk Nederlands Meteorologisch Institutt, Mededelinger En Verhandelingen, No. 89, 68 pp.

21. White, W. B., and A. E. Walker, 1973: Meridional Atmospheric Teleconnections Over the North Pacific. Mon. Wea. Rev., 101, No. 11, p. 817-822.

INITIAL DISTRIBUTION LIST

		No. Copies
1.	Defense Documentation Center Cameron Station Alexandria, VA 22314	2
2.	Library, Code 0212 Naval Postgraduate School Monterey, CA 93940	2
3.	Department of Oceanography, Code 58 Naval Postgraduate School Monterey, CA 93940	3
4.	Professor G. Jung, Code 58Jg Department of Oceanography Naval Postgraduate School Monterey, CA 93940	2
5.	Professor R. Elsberry, Code 51Es Department of Meteorology Naval Postgraduate School Monterey, CA 93940	1
6.	Oceanographer of the Navy Hoffman Building No. 2 200 Stovall St. Alexandria, VA 22332	1
7.	Office of Naval Research Code 480 Arlington, VA 22217	1
8.	Dr. Robert E. Stevenson Scientific Liaison Office, ONR Scripps Institution of Oceanography La Jolla, CA 92037	1
9.	Library, Code 3330 Naval Oceanographic Office Washington, DC 20373	1
10.	SIO Library University of California, San Diego P.O. Box 2367 La Jolla, CA 92037	1

No. Copies

11. Department of Oceanography Library — 1
University of Washington
Seattle, WA 98105

12. Department of Oceanography Library — 1
Oregon State University
Corvallis, Oregon 97331

13. Commanding Officer — 1
Fleet Numerical Weather Central
Monterey, CA 93940

14. Commanding Officer — 1
Environmental Prediction Research Facility
Naval Postgraduate School
Monterey, CA 93940

15. Department of the Navy — 1
Commander Oceanographic System Pacific
Box 1390
FPO San Francisco 96610

16. Mr. Sigurd Larson — 2
Environmental Prediction Research Facility
Naval Postgraduate School
Monterey, CA 93940

Thesis 157210
L2743 Larson
c.1
A statistical verification of a ten year series of computed surface wind conditions over the North Pacific and North Atlantic Oceans.